FAULT LOCATION IDENTIFICATION FOR A VSC-HVDC SYSTEM WITH A LONG HYBRID TRANSMISSION MEDIUM

by

Hashim Abbas M. Al Hassan

Bachelor of Science in Electrical Engineering, University of Pittsburgh, 2010

Submitted to the Graduate Faculty of

Swanson School of Engineering in partial fulfillment

of the requirements for the degree of

Master of Science

University of Pittsburgh

2014

UNIVERSITY OF PITTSBURGH

SWANSON SCHOOL OF ENGINEERING

This thesis was presented

by

Hashim Al Hassan

It was defended on

March 03, 2014

and approved by

Gregory F Reed, PhD, Associate Professor, Electrical and Computer Engineering Department

Zhi-Hong Mao, PhD, Associate Professor, Electrical and Computer Engineering Department

Thomas McDermott, PhD, Assistant Professor, Electrical and Computer Engineering Department

Thesis Advisor: Gregory F Reed, PhD, Associate Professor, Electrical and Computer Engineering Department

FAULT LOCATION IDENTIFICATION FOR A VSC-HVDC SYSTEM WITH A LONG HYBRID TRANSMISSION MEDIUM

Hashim A. Al Hassan, M.S.

University of Pittsburgh, 2014

Electrical energy transmission technologies are evolving as the need for sustainable energy resources continues to increase. HVDC transmission systems are becoming more prominent in power system design and operation, due to their superior performance in transmitting large amounts of power over long distances, which is needed in applications such as offshore wind farm developments. Research activities for HVDC systems are being pursuit to further improve their operation, reliability, quality, and costs. One particular aspect of improving HVDC systems is the efficient and economic maintenance of the system during post-disturbance conditions, which makes the problem of identifying the exact fault location on the line a critical issue. Fault location can be determined by using fault locators, which rely on sending a signal and using the reflected wave of that signal to determine the exact fault location. However, fault locators may cause further damage to the line and lack the ability to locate temporary faults. Locating temporary faults could be useful in determining weak points of the system, in order to do preventative maintenance, which improves the reliability of the system. Therefore, the technique of locating faults using fault transient data has emerged. Also, fault locators lack the ability to locate faults in a hybrid DC line system, where the transmission medium consists of segments of both underground cables and overhead lines, when using only terminal measurements. Therefore, solving the fault location problem utilizing transient data recorded at the terminals in systems of

two and three different transmission medium segments is investigated in this thesis for an HVDC system with voltage source converters (VSC), as a means to demonstrate improved post-disturbance efficiency.

TABLE OF CONTENTS

LIST OF TABLES

LIST OF FIGURES

ACKNOWLEDGMENTS

First of all, I would like to thank God for the gifts that he has given me, the lessons he has taught me and for the guidance that has been provided from him. Also, I would like to say that there is no way that I could properly and sufficiently thank God for the many blessings that I have not been fully appreciative of.

Then, I would like to thank my parents for their continuous support and encouragement, that without, I would not have been where I am today. They have always encouraged me to earn the highest degree and instilled in me the love of acquiring knowledge. To be specific, I would like to thank my mom for her enormous love and for instilling in me the desire for high achievements from a very young age. Besides that, my father has been of valuable intellectual knowledge and support that helped me plan and continue my higher education. Specifically, he taught me important life and academic skills such as good planning, time management, and critical thinking.

Second, I would like to thank my loving wife Ola for her support and for providing me with so much love and warmth that helped me to be more focused and assured. I would also like to thank her for providing a relaxing and comforting home for me, which was essential for my success. Ola has also provided me with the motivation to be the best I can and to improve, not just academically but in all aspects of my life such as personal, social, and spiritual.

In addition, I would like to thank my brother Ali for his support while I am here in the United States and for always being and standing up with. I also, would like to thank my sisters Sabreen and Amal for their love, support and encouragement and would like to thank my other brothers Mohammed and Ahmed for their love and respect.

I would like also to thank my graduate research advisor Professor Gregory Reed for his support and for pushing me not just to grow technically but also to develop and grow professionally and personally. He has been an invaluable resource for me to help me understand the business and practical side of engineering. He pushed me and provided me with opportunities to work on practical projects, develop essential life and professional skills such as networking, communication, and leadership. I also would like to thank Professor McDermott for his valuable technical advice and for his support. I would also like to thank Professor Kusic for supporting me and providing me with technical expertise. Finally, I would like to thank Professor Mao for his invaluable advice, motivation, and encouragement.

I would like also to give special thanks to my colleague Brandon Grainger for the enormous amount of advice and lessons that he taught me and would like to thank my friend and former colleague Dr. Hussain Bassi for the critical lessons that he taught me and for inspiring me to continue my education. I also would like to thank my other graduate student colleagues for their support and help, in no particular order, Mathew Korytowski, Emmanuel Taylor, Rusty Scioscia, Alvaro Cardoza, Bob Kerestes , Ansel Barchowsky, and Patrick Lewis.

Hashim A. Al Hassan

1.0 INTRODUCTION

One of the greatest engineering achievements of the 20th century - the U.S. electric power grid - is facing a threatening challenge. The power grid is starting to become obsolete in its design operation, as it is aging very fast due to our growth in population and our increasing dependence on electricity. In addition, the majority of the bulk transmission grid in the U.S. is aging, much of it dating back to well over 50 years or more. According to a DOE document published in 2008 [1], our demand for electricity is expected to grow 30% by 2030. Also, the cost for new generation and transmission is climbing sharply, and an investment of approximately $1.5 trillion will be required over the next 20 years to pay for the necessary infrastructure upgrades alone [1]. Therefore, the United States has developed policies to tap into the potentials of renewable energy resources such, as the goal of implementing 20% wind energy by 2030 [2]. Also, The U.S. has established policies to support the modernization of the electricity transmission and distribution system to maintain secure and reliable electricity infrastructure that meets the expected demand growth of the future.

This has led utilities, suppliers, and associated researchers to advance High Voltage Direct Current (HVDC) technology as an enabler to exploit more renewable energy resources, which is a vital element in the move toward the grid of the future. Transmitting large amounts of renewable energy such as wind over long distances onshore and offshore economically and efficiently is critical to supporting the energy needs of the future. Thus, Voltage Source

Converter based HVDC systems (VSC-HVDC) have emerged as an enhanced technical approach over conventional HVDC systems. VSC-HVDC is used in applications such as long distance transmission, isolating AC grids, and connecting offshore wind to the grid. The VSC-HVDC system is a very practical technology in transmitting large amounts of wind power from the ocean to land over long distances [3]. Also, using submarine cables at sea in conjunction with overhead transmission lines on land as the transmission medium is a practical way to connect a wind farm station offshore to an onshore station. That is especially the case when the onshore station lies at a very far distance from the coastline. When cable or line faults occur in such systems, it is critical to apply the necessary action to restore the service in the fastest and most economical possible way. Also, it is beneficial to be able to locate temporary faults, which help the operating company perform preventative maintenance on such systems. Therefore, it is critical to have a very effective tool for locating cable and line faults in order to minimize maintenance cost, and increase operational reliability.

1.1 PROBLEM STATEMENT

The fault location identification issue of transmission systems is a continually evolving problem. Currently, there are multiple methods to locate faults for high voltage AC (HVAC) transmission systems [4, 5], and Line Commutated Converter based HVDC systems (LCC-HVDC) [6-9] for either cables or overhead lines using terminal measurements. The authors in [6] have dealt with the non-homogenous case with LCC converters. The most common and most practical method for fault location is the use of the traveling wave principle. This method has not been thoroughly investigated with VSC-HVDC systems. Researchers always need to investigate different line

terminations because line termination plays a role in changing the shape of the traveling wave surge, which could make the fault location mission either easier or more difficult [10]. Therefore, the author in [10], has investigated the fault location problem in a VSC system with a homogenous transmission medium consisting of either cable or overhead line. However, the fault location problem for non-homogeneous transmission systems, where the transmission medium consists of sections of different characteristics has not been thoroughly investigated for all systems. The authors in [11] have investigated fault location for HVAC systems consisting of cables and overhead line segments. Also, the authors in [6] have investigated fault location for LCC-HVDC systems with segments of overhead lines and cables. However, the scientific community lacks thorough research for locating faults in a VSC-HVDC system with nonhomogeneous sections. Therefore, an attempt is made in order to thoroughly investigate and solve this problem for a system that consists of two non-homogenous sections as shown in Figure 1.1and three sections as shown in Figure 1.2.

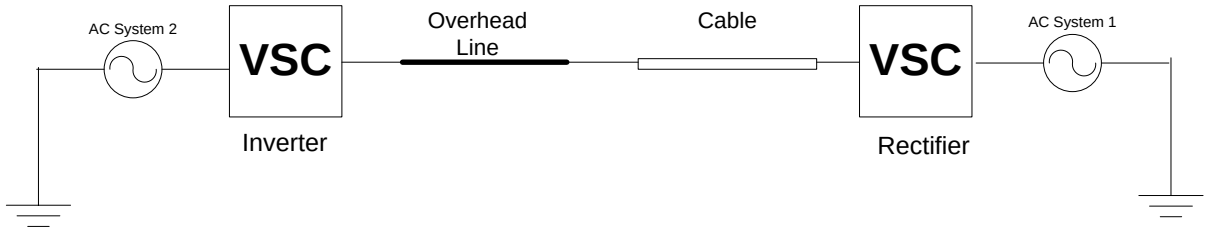

Figure 1.1 VSC-based HVDC transmission system with two non-homogenous sections (hybrid 2-segment)

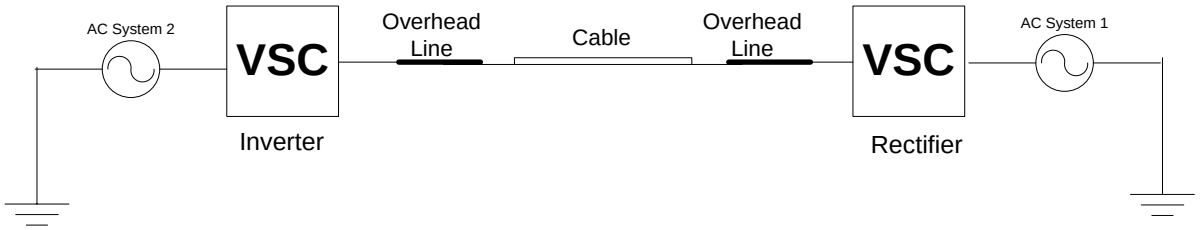

Figure 1.2 VSC-based HVDC transmission system with 3 non-homogenous sections (hybrid 3-segment)

1.2 MOTIVATION

HVDC transmission systems are becoming more prominent in power system design and operation, due to their superior performance in transmitting large amounts of power over long distances, which is needed in applications such as offshore wind farm developments . Research activities for HVDC systems are being pursuit to further improve their operation, reliability, quality, and costs. One particular aspect of improving HVDC systems is the efficient and economic maintenance of the system during post-disturbance conditions, which makes the problem of identifying the exact fault location on the line a critical issue.

Before the advent of fault locators, when a permanent fault occurred on the lines of a transmission system, patrol units were dispatched to locate the fault visually, which could take many hours for long lines depending on the line length and the location of the fault. Alternatively, fault location could be determined through the use of fault locators which rely on sending a signal and using the reflected wave of that signal to determine fault location.

However, these fault locators may cause further damage to the line and also lack the ability to locate temporary faults. Locating temporary faults could be useful to determine weak points in the system and help rectify them through preventive maintenance measures, which in turn provide improved system reliability.

In the case of when underground cables are the transmission medium, fault location can not be done visually. Also, currently there are gaps in the fault location problem, especially when

it comes to non-homogenous HVDC systems. Therefore, an attempt is made in order to fill in the gaps of the problem of fault location, and improve the operation and protection of commonly used HVDC systems.

2.0 FAULTS BACKGROUND

2.1 INTRODUCTION

This section presents the basic background necessary in order to investigate the fault location problem. Methods and information are presented for AC systems because AC systems are a more mature technology. Then the DC systems are investigated. First, fault types for AC systems are presented. After that, HVDC configurations are presented. Then, DC fault types are presented. Finally, the traditional fault location methods are presented.

2.2 HVAC FAULT TYPES

All different faults for three phase systems along with a basic explanation for each case are presented in this section. The information in this section is from [12] and [13]. More details are found in these books.

2.2.1 Single Phase-To-Ground Fault

A single phase-to-ground fault occurs when a connection between a single phase and the ground is established. This could happen due to lighting or when a conductor makes contact with grounded structures. Figure 2.1 shows this fault occurring at point p with fault impedance Z_f.

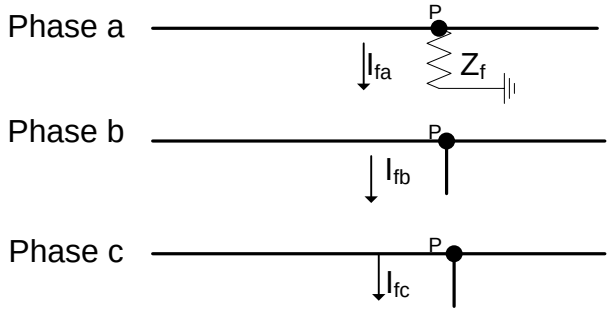

Figure 2.1 Diagram for a single-phase-to-ground fault at p of phase a with impedance Zf

2.2.2 Phase-To-Phase Faults

A line-to-line fault occurs when a connection is established between two phases as shown in Figure 2.2

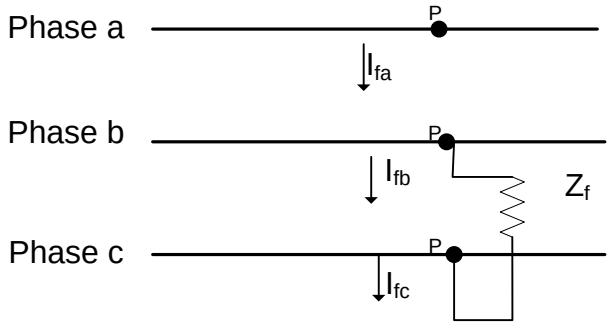

Figure 2.2 Diagram for a line-to-line fault at p between phases b and c with impedance Zf

2.2.3 Phase-To-Phase-To-Ground Faults

This condition occurs when a connection between two of the phases and ground are established so that current path is redirected through the ground from both phases as shown in Figure 2.3.

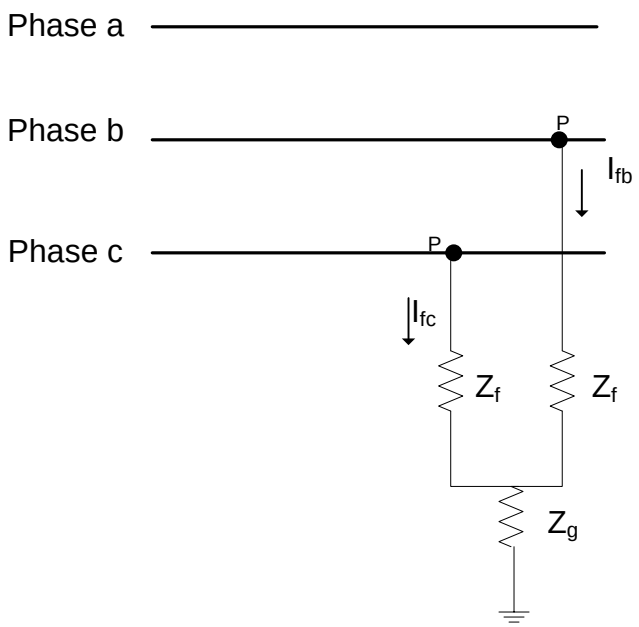

Figure 2.3 Diagram for a line-to-line-to-ground fault at p between phases b and c with impedances Zf

2.2.4 Three-Phase Fault

This fault occurs when a contact is established between all the phases. Figure 2.4 shows this type of fault.

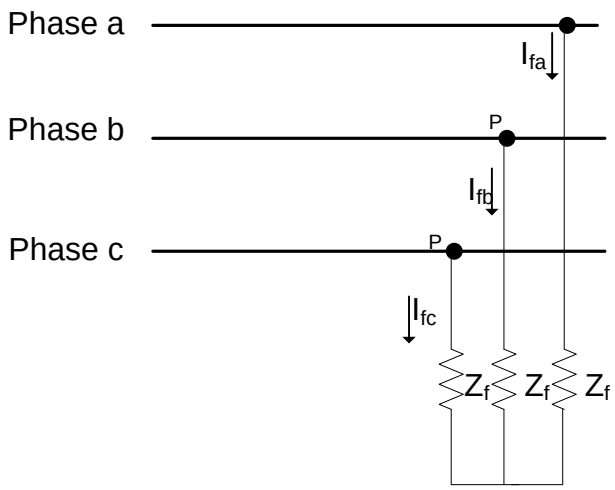

Figure 2.4 Diagram for a three-phase fault

2.2.5 Three-Phase-To-Ground Fault

Three-phase-to-ground faults occur the same way as three-phase faults except this time a path to ground is established as well. Figure 2.5 shows this type of fault.

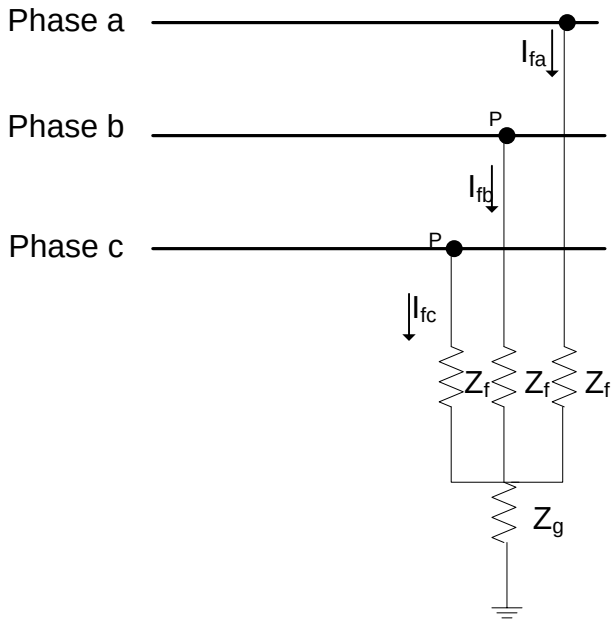

Figure 2.5 Diagram for a three-phase-to-ground fault

2.2.6 Broken-Conductor Fault

A broken-conductor or open-circuit fault is shown in Figure 2.6 for one phase. This fault can also occur for multiple phases.

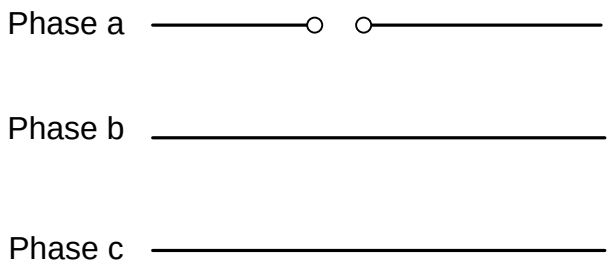

Figure 2.6 Diagram for an open conductor fault

2.2.7 Phase-To-Ground Fault with Broken Conductor

This type of fault occurs when a short-circuit-to-ground fault along with an open-conductor fault occur at the same time. Figure 2.7 shows this type of fault. For this case, assuming that the measurement is taken from the left then the open conductor is outside of the measurement loop.

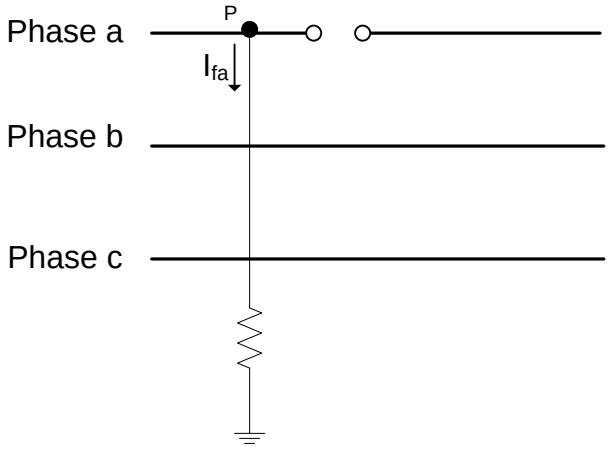

Figure 2.7 Diagram for an open conductor fault

2.2.8 Broken Conductor with Phase-To-Ground Fault

This type is a characterization of the fault of figure 8 when the measurement is taken from the right.

2.2.9 Multiple Faults Occurring Simultaneously

This occurs when more than one type of faults occur with another simultaneously such as the occurrence of a single-phase-to-ground fault combined with a line-to-line fault.

2.2.10 Double Faults

These are single-phase-to-ground faults occurring at two different locations. They could be in one circuit or multiple circuits. These are also called cross-country ground faults.

2.2.11 Flashover Faults

Lighting strikes to a ground wire or tower on a double circuit line cause this type of fault. It could also be caused by a direct strike to a phase conductor.

2.2.12 Inter-System Faults

When a fault occurs at transmission lines hung on the same tower but rated at different voltages, they are called inter-system faults.

2.3 HVDC TRANSMISSION SYSTEM CONFIGURATIONS

The following figures show the different configurations of two main topologies (Monopolar and Bipolar) HVDC transmission systems. For more information see [14].

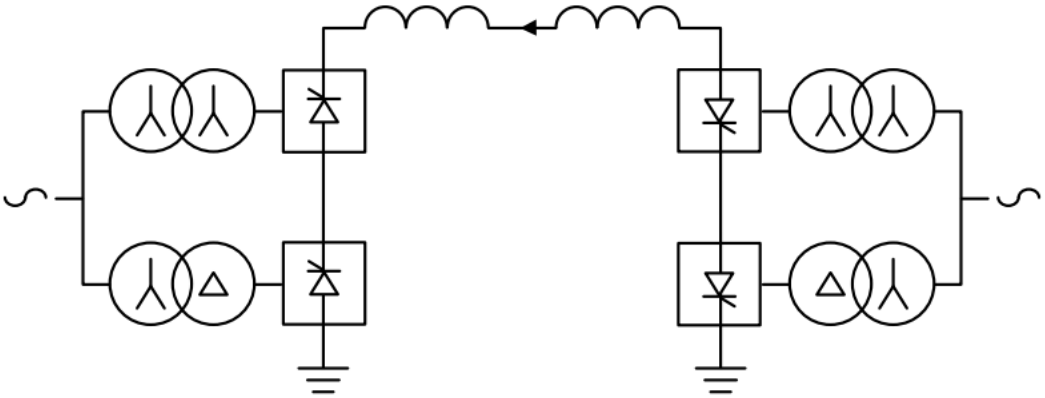

Figure 2.8 Monopolar HVDC transmission system with ground return [14]

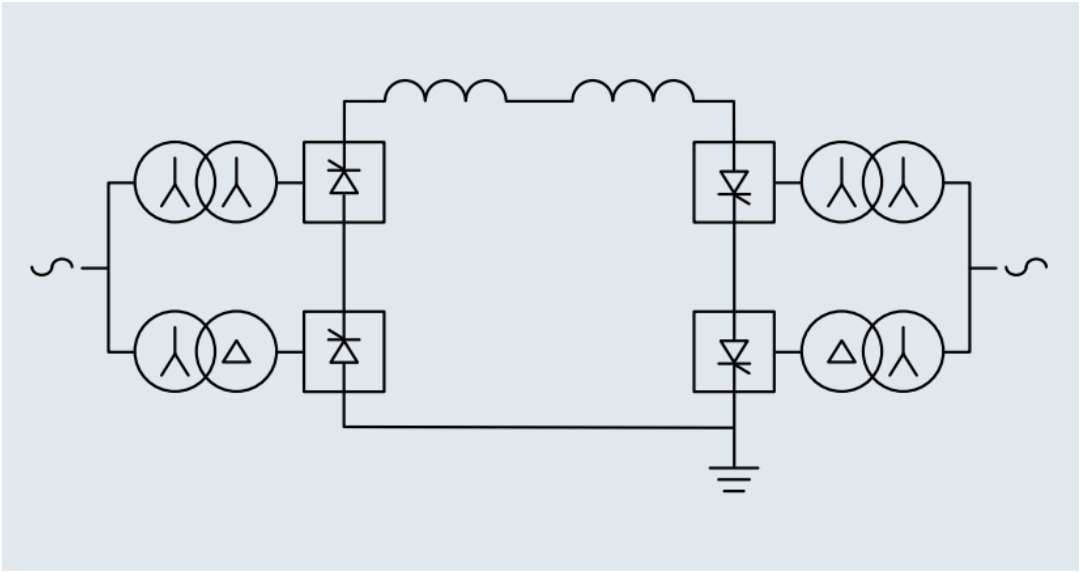

Figure 2.9 Monopolar HVDC transmission system with medium voltage metallic return [14]

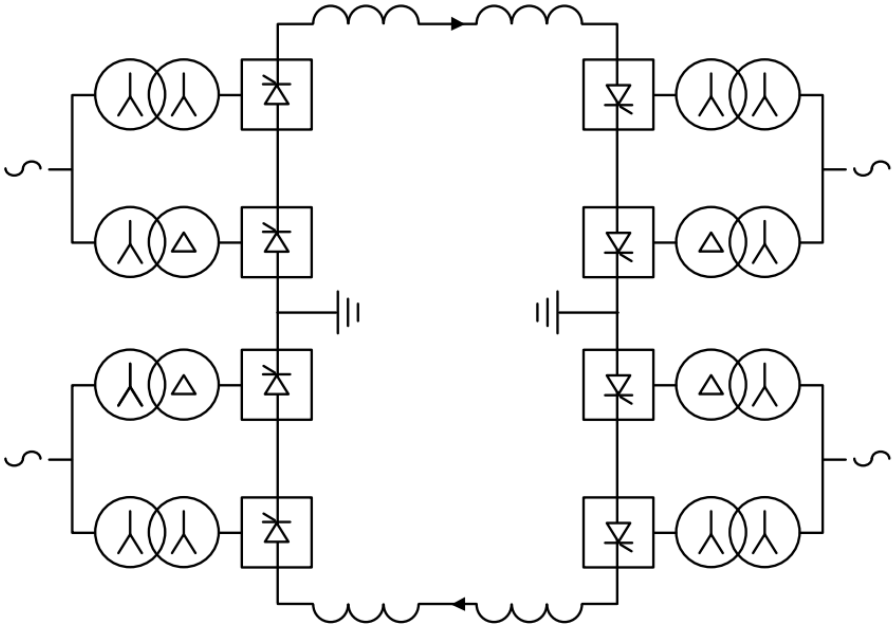

Figure 2.10 Bipolar HVDC transmission system [14]

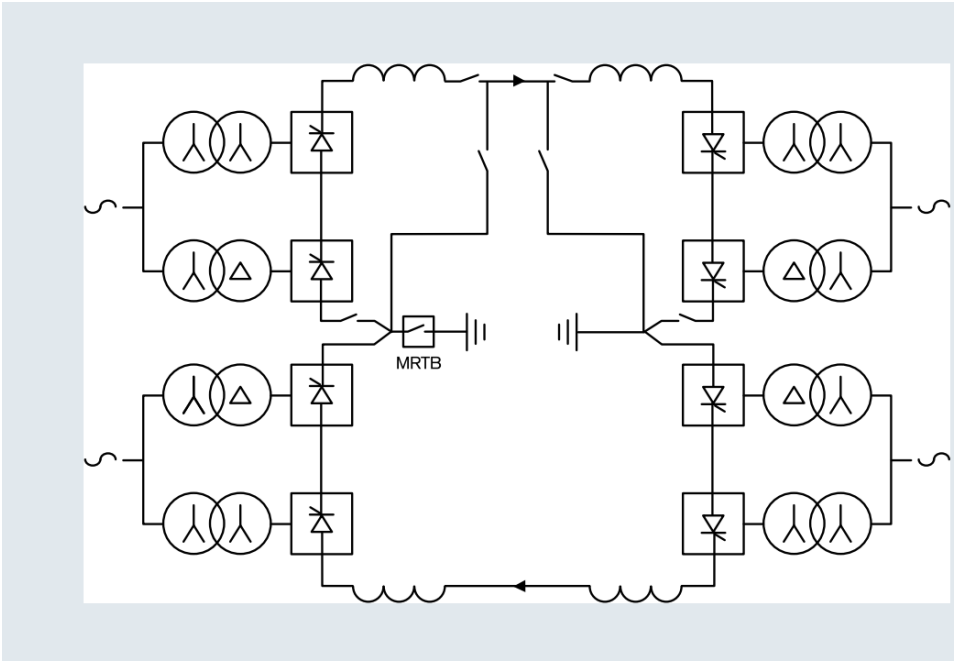

Figure 2.11 Bipolar HVDC transmission system with monopolar metallic return for pole outage [14]

2.4 HVDC FAULT TYPES

2.4.1 Single Pole-to-Ground Fault

A pole-to-ground fault occurs when one of the poles (positive or negative) is short circuited with the ground. When this occurs for a bipolar system, only the faulted pole is shut down, while the other pole continues conducting using the ground as a return. This allows the system to transfer half the power it was previously transferring. If the system is a monopolar instead of a bipolar system, the system is shut down and no power is transferred. Figure 2.12 shows this type of fault on a monopolar system.

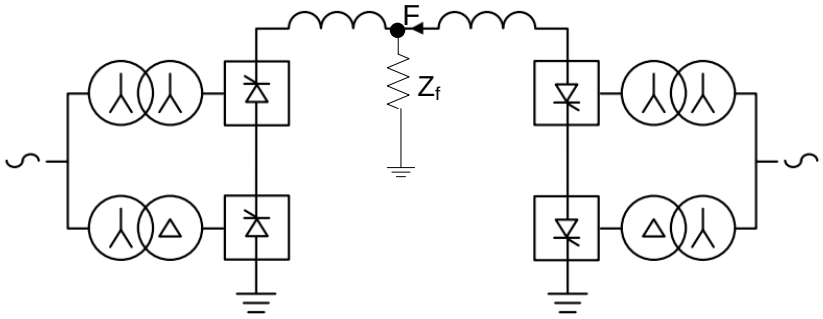

Figure 2.12 A single pole-to-ground fault on a monopolar system

2.4.2 Pole-to-Pole Fault

This fault occurs only for a bipolar system and it occurs when the two poles are short circuited. A complete shutdown of the system is required when this happens. Figure 2.13 shows this type of fault.

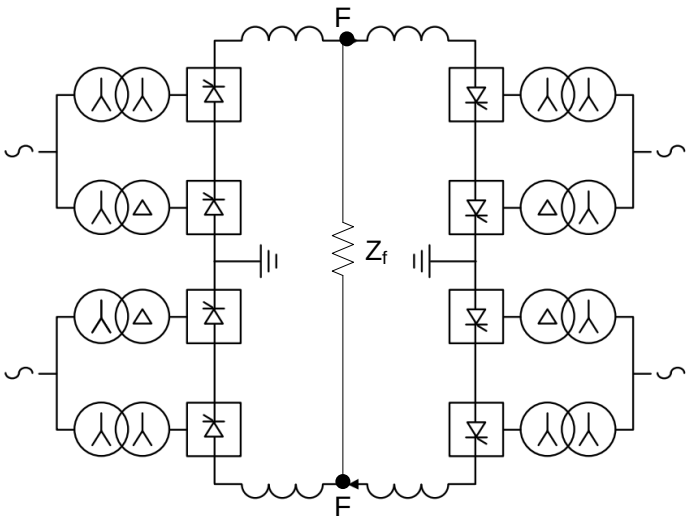

Figure 2.13 A single pole-to-pole fault on a bipolar system

2.4.3 Pole-to-Pole-to-Ground Fault

This type of fault occurs when the two poles of a bipolar system are short circuited through the ground. A complete shutdown of the system is required for this type of fault. Figure 2.14 shows this type of fault.

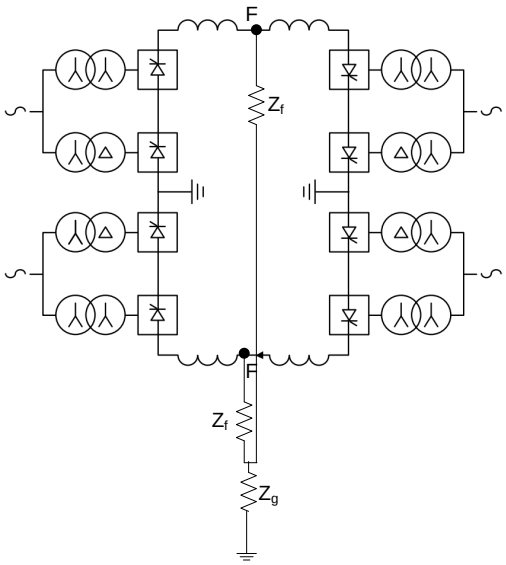

Figure 2.14 A single pole-to-pole-to-ground fault on a bipolar system

2.4.4 Other Types of HVDC Faults

Other types of HVDC faults occur in a similar manner as AC systems faults such as double faults, multiple faults and flashover faults.

3.0 FAULT LOCATION METHODS

Fault location is a growing research topic due to the increased demand of high power quality and continuous power supply. Transmission line fault location methods have been considered more critical than distribution system faults because transmission lines are generally long and it could take the maintenance crew a couple of hours to locate a permanent fault .This could lead to a large economic loss and it could also lead to further problems on the power system. Also, it is beneficial to determine the location of temporary faults in order to apply the necessary action to prevent the recurrence of those faults. However, the maintenance crew might not be able to locate these faults by visual inspection Also, modern fault locators cannot locate temporary faults because they rely on sending a signal offline on the damaged cable. Therefore, finding the location of temporary fault can only be done by investigating the transient data recorded during and after the fault. Therefore, fault location methods using transient data recorded on the terminal is a useful technology that would provide cheap and efficient maintenance of the power system by reducing outage time besides protecting the power system from potential damage.

There has been a significant amount of research for locating faults in HVAC transmission systems [4,11,13,15]. Also there has been a lot of research on HVDC fault location technology [6-10]. However, HVDC fault location technology has some gaps, which we attempt to fill in this thesis. However, before doing so, a survey into the current technology has to be done. This

will be done for AC systems since it is a more mature technology and the general theories that are used in AC fault location methods are very similar to those for DC systems. Then a method will be proposed for a hybrid HVDC system with VSC units as the terminal units.

In this section, the traditional fault location methods along with their measurement techniques are presented. These include one-terminal measurement methods, two-terminal measurement methods, impedance methods, traveling wave methods, high-frequency methods and machine learning methods. A focus will be given to the traveling wave method since it is the method that is used in this thesis.

3.1 ONE-ENDED IMPEDANCE BASED TECHNIQUES

This technique uses measurements of line-to-ground voltages and currents of all phases at one end of the line in order to estimate the apparent impedance which is used for pinpointing the fault location of any type of fault [4]. Phase-to-phase faults can be located using only line-to-line voltages, and the location of line-to-ground faults can be estimated with the use of source impedance. Table 1 shows the impedance calculations for estimating fault location if the fault resistance is ignored [4].

Table 1. Simple impedance equations [4]

Fault type	Positive-sequence impedance equation (mZ_{1L}=)
a-ground	$V_a/(I_a + kI_R)$
b-ground	$V_b/(I_b + kI_R)$

Table 1 (continued)

c-ground	$V_c /(I_c + kI_R)$
a-b or a-b-g	V_{ab} / I_{ab}
b-c or b-c-g	V_{bc} / I_{bc}
c-a or c-a-g	V_{ca} / I_{ca}
a-b-c	Any of V_{ab} / I_{ab}, V_{bc} / I_{bc}, V_{ca} / I_{ca}

Where

$$k = (Z_{0L} - Z_{1L}) / 3Z_{1L} \tag{3.1}$$

Z_{0L} is the zero-sequence line impedance, m is the per unit distance to fault, and I_R is the residual current. There are many factors, that are not represented by the equations in Table 1 which effect the accuracy of the fault location estimate [4] . Some of these factors are: fault resistance which is high for ground faults (the majority of faults on overhead transmission lines), inaccurate fault type identification, inaccurate zero-sequence impedance, presence of shunt reactors, measurement errors and many others [4].

To enhance fault location estimates more information about the system is necessary. For the implementation of the one-ended fault location methods, the following data are necessary: [4]

1. Phase-to-ground voltages and phase currents.
2. Identifying the fault type.
3. Pre-fault data are required for some methods.

This method uses the following equipment to obtain and process data [4]:

1. A microprocessor-based relay or other three-phase voltages and currents measurement device that could calculates fault location estimates.
2. Communication medium or SCADA interface for remote calculation of fault location estimates.

3.1.1 Accounting for Main Sources of Error: Fault Resistance and Load

In order to determine an accurate fault location equation, the circuit in Figure 3.1 is examined.

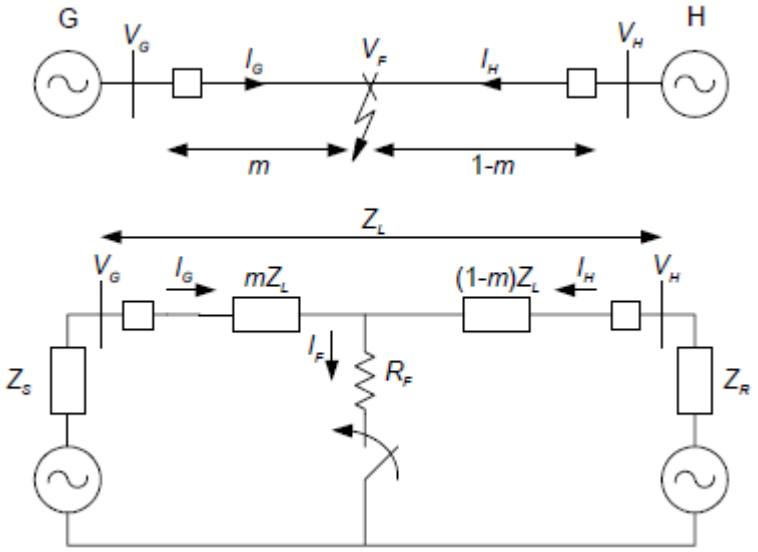

Figure 3.1 One-line diagram and equivalent circuit for a three-phase fault on a transmission line with two sources, G and H [4].

Figure 3.1 shows a fault on a homogenous transmission line with fault resistance R_F and a line impedance Z_L between terminals *G* and *H*. The remote and local terminals are represented by their Thevenin equivalents. From Figure 3.1 it can be easily seen that the voltage drop from terminal *G* due to the fault occurring at location *m* per unit is:

$$V_G = mZ_L I_G + R_F I_F \tag{3.2}$$

Where

V_G is the voltage at terminal G.

m is the per unit distance to the fault.

Z_L is the line impedance between terminals G and H.

I_G is the line current from terminal G.

R_F is the fault resistance.

I_F is the total fault current.

The impedance measured from terminal G can be found by dividing (3.2) by I_G:

$$Z_{FG} = \frac{V_G}{I_G} = mZ_L + R_F \frac{I_F}{I_G} \tag{3.3}$$

Where Z_{FG} is the apparent impedance measured from G to the fault. The fault impedance will have a reactive component if the ratio $\frac{I_F}{I_G}$ is complex. This reactive component can be inductive or capacitive depending on the angle of the ratio. The reactive component will be zero when the angle is zero. That is when I_H is zero, or is in phase with the local current, I_G. The reactive component could potentially lead to an error in estimating fault location as shown in Figure 3.2 [4].

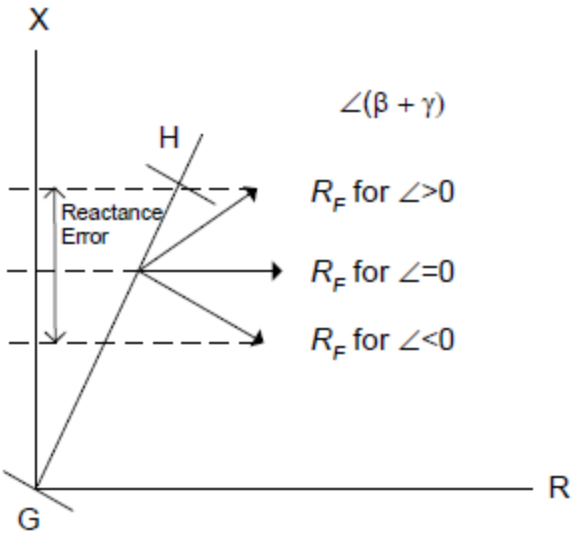

Figure 3.2 Representation of fault resistance and pre-fault load errors [4].

Now, In order to analyze the parameters effecting the error, we need to consider the parameters effecting the angle of $\frac{I_F}{I_G}$. To do that, we need to consider the pre-fault system. Let us define the following equation.

$$\Delta I_G = I_G - I_L \tag{3.4}$$

Where:

ΔI_G is the difference current

I_L is the pre-fault load current.

And we write equation (3.3) as:

$$Z_{FG} = \frac{V_G}{I_G} = mZ_L + R_F \frac{1}{d_s n_s} \tag{3.5}$$

Where

d_s is the current distribution factor in equation (3.6)

n_s is the circuit loading factor in (3.7).

$$d_s = \frac{\Delta I_G}{I_F} = \frac{Z_H + (1-m)Z_L}{Z_H + Z_L + Z_G} = | d_s | \angle \beta \tag{3.6}$$

$$n_s = \frac{I_G}{I_G - I_L} = \frac{I_G}{\Delta I_G} = | n_s | \angle \gamma \tag{3.7}$$

If the system is homogenous then β is zero. If there is load flow on the system then γ won't be zero. If the magnitude of the fault current I_G is much greater than the magnitude of the load current, I_L, then, γ will approach zero. The sum of the angles β and γ, determines the reactive component of caused by the fault resistance R_F [4].

In order to implement fault location algorithms, some simplifying assumptions have to be made in order to reduce the effect of R_F. The performance of such an algorithm will depending on the underlying assumptions. The following section describes such an implementation of the algorithm.

3.1.2 Algorithms

(a) Simple Reactance Method

This method compensates for the fault resistance by taking only the imaginary part of the apparent impedance measurement. The fault locator uses the fact that the distance to the fault is proportional to the ratio of the measured reactance to the reactance of the entire line. The per unit distance to the fault is:

$$m = \frac{\mathrm{Im}(V_G / I_G)}{\mathrm{Im}(Z_L)} \tag{3.8}$$

The line-to-ground fault location is:

$$m = \mathrm{Im}\left[\frac{V_{Ga}}{I_{Ga} + k_0 I_R)}\right] / \mathrm{Im}(Z_{1L}) \tag{3.9}$$

Where

$$k_0 = (Z_{0L} - Z_{1L}) / 3Z_{1L} \tag{3.9}$$

The residual current is

$$I_R = 3I_0 \tag{3.10}$$

The algorithm can introduce large reactance error when the fault resistance is high as shown in Figure 3.2. The error is zero for zero fault resistance or if I_G and I_F are in phase.

(b) A Method without Using Source Impedances

If the load current is eliminated by finding the change in current on the occurrence of a fault, the above method can be improved. This method has been investigated by many researchers [4]. Using the superposition current ΔI_G, equation (3.2) can be written as:

$$V_G = mZ_{1L} I_G + R_F \frac{\Delta I_G}{d_s} \tag{3.11}$$

Where d_s is the voltage drop across the fault resistance [4]. Multiplying (3.11) by the complex conjugate, ΔI_G^*, using only the imaginary part, we obtain equation (3.12) [4]:

$$\mathrm{Im}(V_G \Delta I_G^*) = m\,\mathrm{Im}(Z_L I_G \Delta I_G^*) + R_F\ \mathrm{Im}(\frac{1}{d_s}) \tag{3.12}$$

For a homogenous system, the angle is about zero for the current distribution factor ($Im(1/d_s)=0$),and the fault location is:

$$m = \frac{\mathrm{Im}(V_G \Delta I_G^*)}{\mathrm{Im}(Z_L I_G \Delta I_G^*)} \tag{3.13}$$

For a nonhomogenous system, an angle correction (β) derived from the source impedance to account for the non-zero current distribution factor in this type of system [4], and the fault location is

$$m = \frac{\mathrm{Im}(V_G I_R^* e^{-j\beta})}{\mathrm{Im}(Z_{1L} I_G \Delta I_R^* e^{-j\beta})} \tag{3.14}$$

The fault location estimate is improved here by reducing the effect of the reactance error. For more details see [1].

(c) Method Using Source Impedances

Knowledge of the source impedance is required when the distribution factor is discounted and when using the positive-sequence model of the line. The fault location can be determined without assumptions using the following quadratic equation [4]:

$$m^2 - mk_1 + k_2 - k_3 R_F = 0 \tag{3.15}$$

Where k_1, k_2 , and k_3 are complex functions of voltage current and source impedances. Equation (3.15) is separated into real and imaginary components in order to have two equations with two unknowns m and R_F and then the equation can be solved.

3.2 TWO-TERMINAL IMPEDANCE BASED METHOD

When data are used from both terminals, fault location equations are calculated in a similar manner as in the previous section. However, now more data are present which allows us to minimize or eliminate the error caused by fault resistance and other factors such as nontranspositions, strong or weak sources, loading and charge current. Also, fault type does not need to be determined in the two-terminal method. The main disadvantage of this method is the

need for a communication channel between both ends and a central unit to process the data [4]. Also, the data recorded needs to be synchronized, which can currently be done using GPS technology. More details on the equipment required for the two-terminal methods will be described later in section 3.3.3.

3.3 TRAVELING WAVE METHOD

This method is based on the traveling wave theory (TWT). Electrical voltage and current is represented by traveling waves and the theory says that whenever a traveling wave hits a junction that wave is reflected and refracted through that junction as illustrated in Figure 3.3. A junction or a discontinuity is a change of impedance, which can be a line termination, a fault point, the point of cable and overhead line interconnection, etc. This can be better understood by making the analogy of sound waves. Sound waves get reflected and refracted through walls, and the sound can be heard as an echo when the waves bounce off the wall with sufficient magnitude. Also, for example, when the wall has sound insulation, the whole wave gets reflected. The insulated wall is equivalent to an open circuit in electric systems.

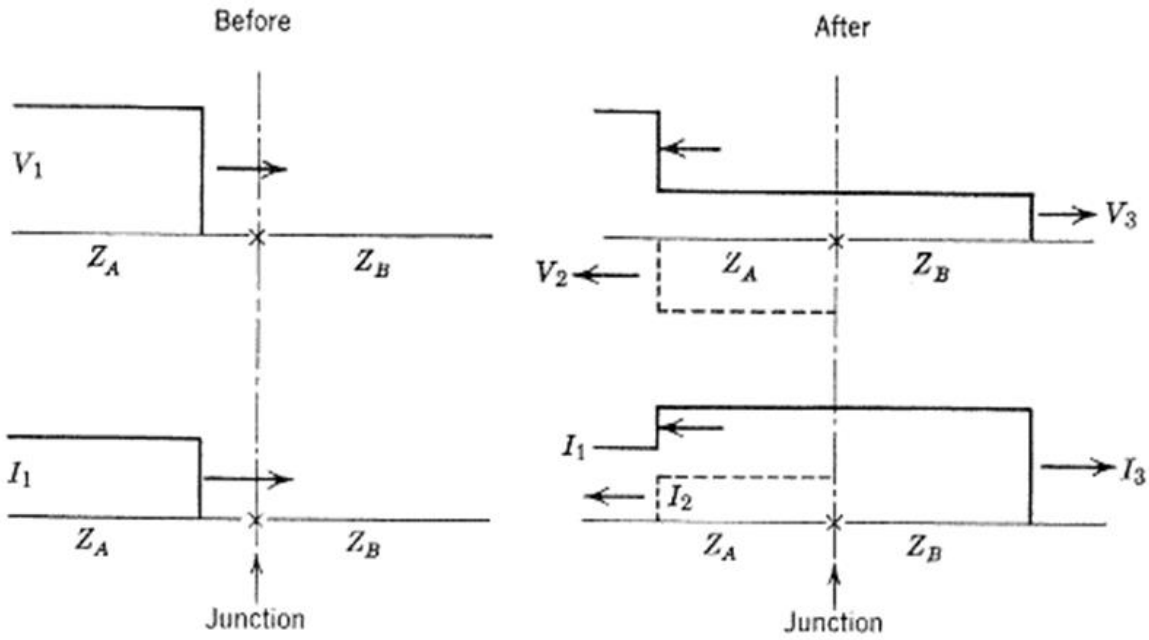

Figure 3.3 A traveling wave being reflected and refracted at a junction [16]

When a fault occurs on a transmission line, a transient wave is initiated that travels back and forth the line at a speed characterized by the transmission line parameters. Therefore, if the travel time was accurately measured, the precise fault location could be estimated. This theory has been in practice for fault location identification on AC cables and overhead lines since 1931 [13]. A decade later the method was widely employed on de-energized underground cables. Utilities have used this method due to its superiority in accuracy over the traditional measured impedance method. Different traveling wave fault location methods were found in the 1950s. In general, these traveling wave methods provided more accurate results at the time than all other methods, but their use became less and less frequent over time because of reliability and maintenance problems. However, recently they have emerged back into the market due to improvements in data acquisition systems, GPS time synchronization, communication systems and the desire for faster and more accurate fault location techniques. The most recent fault

location method using traveling wave theory on overhead lines can be classified into three main categories [13]:

1. Single-ended method using traveling-wave transients caused by the fault.
2. Double-ended method using traveling wave transients caused by the fault.
3. Single-ended method using traveling wave transients caused by circuit-breaker operations.

Traveling wave theory also has three main problems that have to be dealt with which are [13]:

1. The requirement of high sampling frequency rate.
2. The uncertainty in the choice of sampling window.
3. Distinguishing between the traveling wave reflected from the fault point and the wave reflected from the end of the line.

Capturing surge arrival times is the most critical aspect of fault location identification using TWT. Recent advancements in DSP techniques have made this task easier by using techniques such as Discrete Wavelet Transform. Wavelet Transform has been applied in power system analysis for many purposes, such as automatic feature detection, incipient failure detection, and power quality assessment. Another method that relies on a hardware device for capturing surge arrival times is also possible, such as the use of Rogowski Coil.

Fault location using TWT is independent of system network configuration [13]. However, line termination configuration could play a role in changing the shape of the surge. This could in turn make detecting surge arrival time harder or easier depending on the terminal configuration.

3.3.1 Traveling-Wave Fault Location Theory

As mentioned earlier, when a fault occurs on a line, an abrupt injection occurs at the fault point that translates into a traveling wave that travels back to the terminal and bounces back and forth between the terminal and the fault point until it dies out. The fault point and the line termination are considered junctions or discontinuities, which are characterized by a change of impedance, which result in reflections and refractions of the incident wave. This behavior can be visualized better through a lattice diagram as shown in Figure 3.4. The line in the diagram can be a single phase lossless AC line of length l with a characteristic impedance Z_c and a traveling wave velocity v. In Figure 3.4, τ_A and τ_B are the travel times from the fault point to the junction. Also, k_A and k_B, are the reflection coefficients, which are determined by the characteristic impedance rations. The following equations have to be satisfied at any point x [13]:

$$\frac{\partial e}{\partial x} = -L' \frac{\partial i}{\partial t} \tag{3.16}$$

$$\frac{\partial e}{\partial x} = -C' \frac{\partial e}{\partial t} \tag{3.17}$$

Where the resistance is assumed to be negligible and where:

L' is the inductance of the line in per unit length and C' is the capacitance of the line in per unit length.

The solutions of (3.16) and (3.17) are [13]:

$$e(x,t) = e_f(x - vt) + e_r(x + vt) \tag{3.18}$$

$$i(x,t) = \frac{1}{Z_c} e_f(x - vt) - \frac{1}{Z_c} e_r(x + vt) \tag{3.19}$$

Where e_f and i_f are the forward voltage and current, respectively, and e_r and i_r are the reverse voltage and current, respectively. The characteristic impedance of the transmission line is

$$Z_c = \sqrt{\frac{L'}{C'}} \tag{3.20}$$

The velocity of the line is

$$v = \sqrt{\frac{1}{L'C'}} \tag{3.21}$$

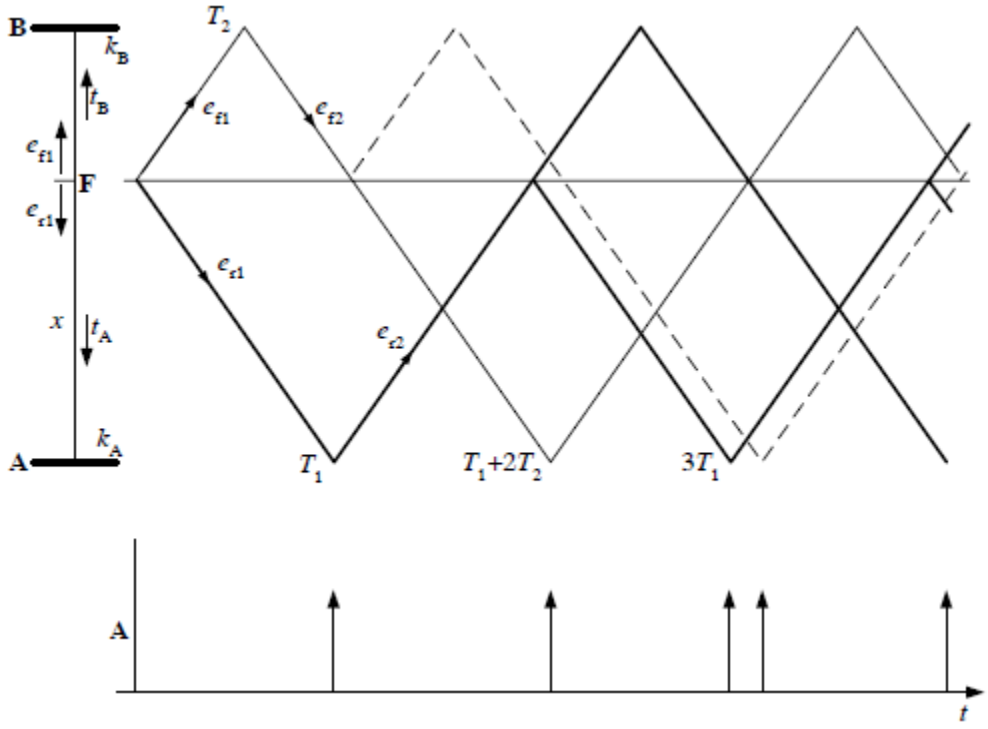

Figure 3.4 Lattice diagram showing traveling wave reflections/refraction for a fault at a distance x from A [13].

The fault distance x measured from terminal A can be calculated easily using equation (3.22) by exploiting GPS technology for time synchronization of measurements at both ends. For three

phase lines, there are three propagation modes when losses are taken into account. Therefore, phase values have to be converted into modal values [13].

$$x = \frac{l - v(\tau_A - \tau_B)}{2} \tag{3.22}$$

3.3.2 Information Required

The traveling wave method depends on knowing the time it takes the surge initiated by the fault to travel from the fault point to the end of the line. That travel time calculation has to be very precise in order to find the fault location precisely [13]. The waves usually travel at around the speed of light for overhead lines and around two thirds of the speed of light for underground cables. Therefore, one way to find the fault distance is by finding the difference between wave arrival times at each end as shown in equation (3.22). Voltage and current waveforms can be used. However, because of buses with lower impedances, the voltage waveform of the traveling surge is reduced. Therefore, it is more practical to use the current waveform especially because the current waveform doubles due to a constant current source [13]. From the above discussion we can summarize the data required as below [13]:

1. A standard time reference at both ends of the line.
2. The appropriate current waveform or the time tag in the voltage method.
3. A method for distinguishing waves.
4. The precise time the traveling wave takes to reach the end of the line.

3.3.3 Equipment Required

The following is the equipment that is necessary to identify fault distances using TWT [4]:

1. A GPS transducer for time synchronization.
2. An appropriate sensor to measure voltage or current depending on the parameter used. For instance, CTs can be used for current measurement.
3. A communication channel such as Ethernet cables to transmit data to a processing station.
4. A computer or a processing chip to process the data and find the fault location.

3.3.4 Accuracy

- Traveling-wave fault locating systems based on GPS technology for AC systems has been shown to have an accuracy of ±300 m, even for very long lines [4].

- Any error in the GPS system will cause errors in the calculated fault location. The Department of Defense of the U.S. has intentionally built a small amount of uncertainty into the GPS system [4].

- Interpreting transients is a major source of error which is caused by many reflected/refracted transients occurring at the same time. This can be caused mostly by lighting strikes because sometimes lighting storms have multiple strikes which results in confusion and more complications [4].

- Voltage transients are damped by stronger buses, which degrade fault location accuracy [4].

- Reasonable transient waveforms are produced by voltage and current transformers [4].

- One-terminal measurement methods require more sophistication as they use the 2nd reflection of the traveling wave and may require signature analysis [4].

3.3.5 Types of the Traveling-Wave Method

Overhead line fault locators are classified into five main types: type A, type B, type C, type D, type E [4]. The following are the explanations of three of those types:

Type A uses one-terminal measurement to locate faults using the first and second reflection of the traveling wave. This type assumes the terminal impedance is much lower than the line surge impedance. This makes up a junction that makes the traveling wave send another reflected wave to the fault point and back to the terminal with sufficient magnitude. It also assumes that the arc fault has a lower effective resistance than the line surge impedance if the fault arc still exists [4]. Finding fault location using this type becomes an issue when there is no total reflection at the fault point, which is a possibility. Also, this type faces problems when the arc extinguishes prematurely because analyzing the transients becomes more difficult [4].

Type D uses two-terminal measurements in which the time difference between the initial surges traveling to each terminal is used to calculate the fault location as in equation (3.22). In this type, many problems associated with the fault location using one terminal measurement are avoided. Some of the problems being avoided are behavior of the arc fault, and discontinuities between two line terminals, such as branches and tapped loads [4]. This type is the one that has been explained in the previous section, and which will be the focus in this research due to its superiority over other methods.

Type E uses one-terminal measurement and the transients created by re-energizing of the damaged line. In [4] it is stated that this method "is equivalent to the Impulse Current Method of fault location widely used on underground cables"

3.4 HIGH-FREQUNCY METHODS

Fault location methods can fundamentally be classified into two main categories. The first one is methods based on measurement of the post-fault line impedance. The second one is methods based on the fault-generated traveling-wave component. Impedance-based measurement fault location methods are limited due to line loading, fault-path resistance and source parameters, etc [13]. The traveling-wave-based fault location methods are limited in AC systems when the fault occurs at a voltage inception close to zero degrees [13]. "For a close-up fault, the time difference between the arrival of the incident wave and the arrival of its reflection from the bus bar will be so short that the waves are unlikely to be detected separately. This could make the interpretation of the information available in the first few milliseconds after the arrival of the first wave front virtually impossible" [13]. Therefore, high frequency transient signals are used to detect the fault location. This method has achieved very high accuracy in determining the fault location [13,22]. In this method, the low fault inception angle is no longer a problem because the high frequency components do not vary with the point on the wave at which the fault occurs [13]. This method was found to be immune to power frequency phenomena such as CT saturation and power swings. Similar methods have also been developed such as the use of wavelet transform to extract the high frequency components of the signal [23]. To achieve higher accuracy, a higher sampling rate should be used [13]. This technique, which is based on high frequency components

of the current and voltage signals, is not widely used because it is expensive and complex " since specially tuned filters for measuring high frequency components is required" [13]. The basic principle of operation relies on first transforming the measured signals using modal transform; then the signals are passed through digital band-pass filters to extract the high-frequency components. Finally, the fault location is determined by finding the time difference between the first and the subsequent surges [13].

3.5 MACHINE LEARNING METHODS

These methods rely on the use of modern machine learning methods such as artificial neural networks (ANN). The methods rely on using test data to train the neural network and then using the trained neural network as a fault location identifier. These methods use the fundamental components of voltages and currents before, during, and after the fault, similar to the impedance based method [24, 25]. Also, the trained ANN is only specific to the system considered.

4.0 FAULT LOCATION UTILIZING TRAVELING WAVE THEORY

The two-ended traveling wave theory method is used here for many reasons. First, it is not affected by the fault resistance or fault type as opposed to the impedance based method. Second, it does not require high computation and complexity as opposed to the high-frequency methods. Third, it is used instead of the machine learning methods because it does not require a lot of test data and it is not very specific to a particular system. In addition, it is very difficult to determine fault location using one-terminal measurement because of the complexity added by junctions on hybrid systems. Furthermore, the traveling wave method on HVDC systems does not suffer the limitation that it suffers on AC systems due to fault inception angle because faults always produce sufficient magnitudes on HVDC systems .Finally, the problem of saturation is solved here by using Rogowski coil instead of current transformers.

In this chapter, the theory and the algorithms used are presented here. The method developed relies on combining the works of [6] and [10]. Rogowski coil proved to be useful as a measurement device to locate faults using traveling wave theory in HVDC systems [10]. Also, the authors in [6] developed an algorithm for the hybrid 3-section system, which is going to be used in this thesis. In addition, a similar algorithm was implemented for the hybrid 2-section system. The method was tested in chapters 6 and 7 for an ideal DC source system and the VSC-HVDC system, respectively.

4.1 FAULT DISTANCE CALCULATION THEORY AND ALGORITHM

In this section, the mathematical background and derivation for the fault location method used in this thesis is presented along with the computer algorithm for systems with one-section transmission medium, two hybrid sections, and three hybrid sections, respectively.

4.1.1 System with One Transmission Section (Cable or Overhead line)

For a fault occurring at F in the first half section of the line as in Figure 4.1, the fault location distance from the left terminal can be calculated using equation (4.1) after determining the arrival time through the use of high precision GPS synchronizers. For a Fault occurring at the second half section of the line, the fault location distance from the left terminal can be calculated using (4.2). The faulted section can be determined by determining the arrival time difference Δt. If Δt is positive, then the fault is in the first half section. If it is negative, then it is in the second half section.

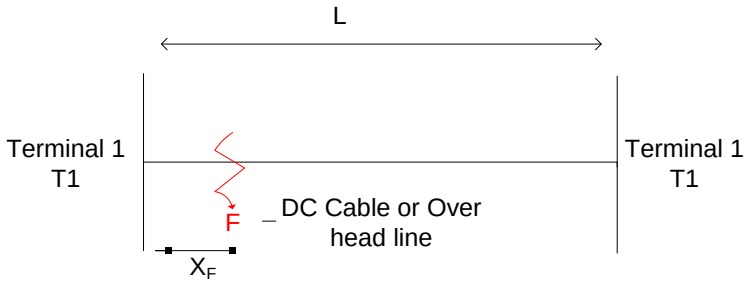

Figure 4.1 Diagram showing a fault on non-hybrid system

$$x_F = \frac{[L-(\Delta t)\times v]}{2} \tag{4.1}$$

$$x_F = L - \frac{[L-|\Delta t|\times v]}{2} \tag{4.2}$$

Where *v* is the speed of the traveling wave and *L* is the length of the cable or overhead line.

4.1.2 Hybrid System with Two Sections (A Cable and An Overhead line)

In this section, a hybrid system consisting of a cable section and an overhead line section is considered as shown in Figure 4.2. This system is more complicated than the previous system because a junction is introduced, which gives the wave increased reflection and refraction at the junction. In addition, the wave propagates at different speeds in the cable and overhead line. This complexity does not affect the first traveling surges. However, the junction affects the subsequent reflections and refractions. Therefore, when we are considering a solution, we need to avoid the use of the second reflections because that would require more computations that are complex.

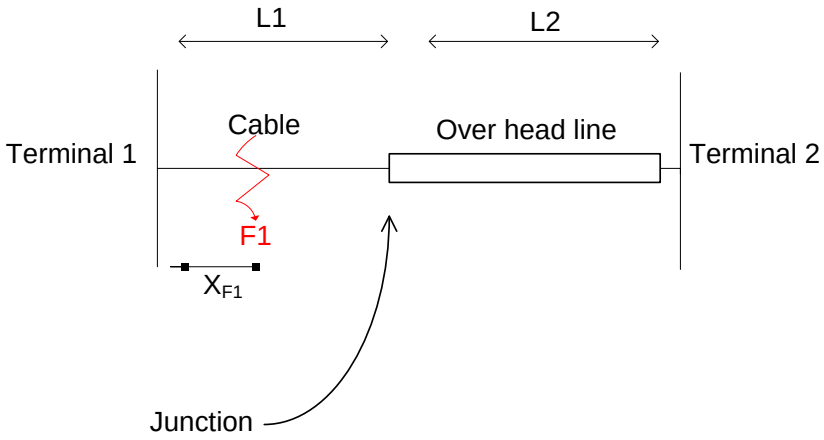

Figure 4.2 Diagram showing a fault on the cable section of a hybrid system

The method that is developed here is similar to the one in the previous section, which uses the measurements from both terminals to the find exact fault location. The equations for this method are derived as follows:

For a fault occuring at the cable junction, the time it takes the surge to travel to terminal 1 is defined by (4.3).

$$t_{1-F1} = \frac{x_{F1}}{v_1} \tag{4.3}$$

Where x_{F1} is the fault location measured from the left for a fault occuring at the cable section and v_1 is the speed of the wave at the cable section. The time it takes the other surge to reach terminal 2 is defined by (4.4)

$$t_{2-F1} = \left(\frac{L_1 - x_{F1}}{v_1} \right) + \frac{L_2}{v_2} \tag{4.4}$$

Where L_1 is the length of the cable section, L_2 is the length of the overhead line section and v_2 is the speed of the wave at the overhead line section . The time diffrence is calculated by (4.5)

$$\Delta t_{12-F1} = t_{1-F1} - t_{2-F1} = \frac{L_1}{v_1} + \frac{L_2}{v_2} - \frac{2x_{F1}}{v_1} \tag{4.5}$$

And the fault location is found using equation (4.6)

$$x_{F1} = \frac{1}{2}(L_1 + \frac{v_1}{v_2} L_2 - \Delta t_{12-F1} v_1) \tag{4.6}$$

For a fault at the overhead line section as shown in Figure 4.3., the derivation is shown below.

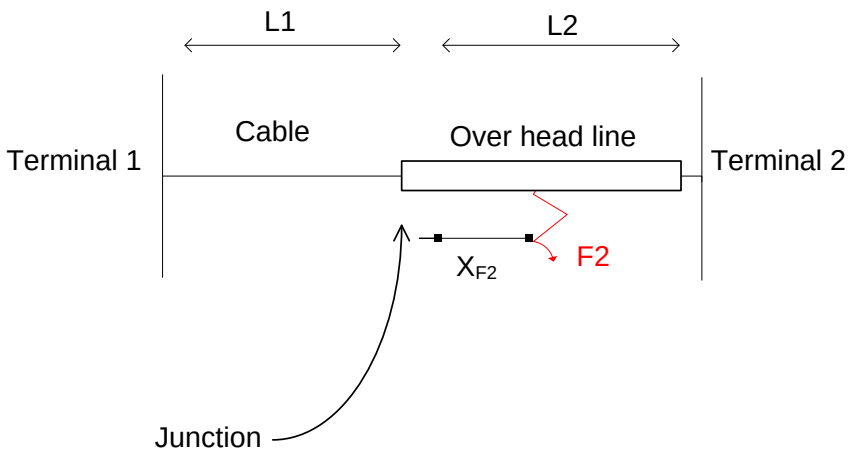

Figure 4.3 Diagram showing a fault on the overhead line section of a hybrid system

The time it takes the surge to travel to terminal 1 is defined by (4.7).

$$t_{1-F2} = \frac{x_{F2}}{v_2} + \frac{L_1}{v_1} \tag{4.7}$$

Where x_{F2} is the fault location measured form the junction for a fault occuring at the overhead line section .The time it takes the other surge to reach terminal 2 is defined by (4.8).

$$t_{2-F2} = \left(\frac{L_2 - x_{F2}}{v_2} \right) \tag{4.8}$$

The time diffrence can be calculated using (4.9)

$$\Delta t_{12-F1} = t_{1-F1} - t_{2-F1} = \frac{L_2}{v_2} - \frac{L_1}{v_1} - \frac{2x_{F2}}{v_2} \tag{4.9}$$

And the fault location is found using equation (4.10)

$$x_{F1} = \frac{1}{2}(L_2 + \frac{v_2}{v_1} L_1 - \Delta t_{12-F2} v_2) \tag{4.10}$$

The algorithm for finding the fault location, which is developed in a similar manner to the algorithm in [6], is shown in the chart in Figure 4.4.

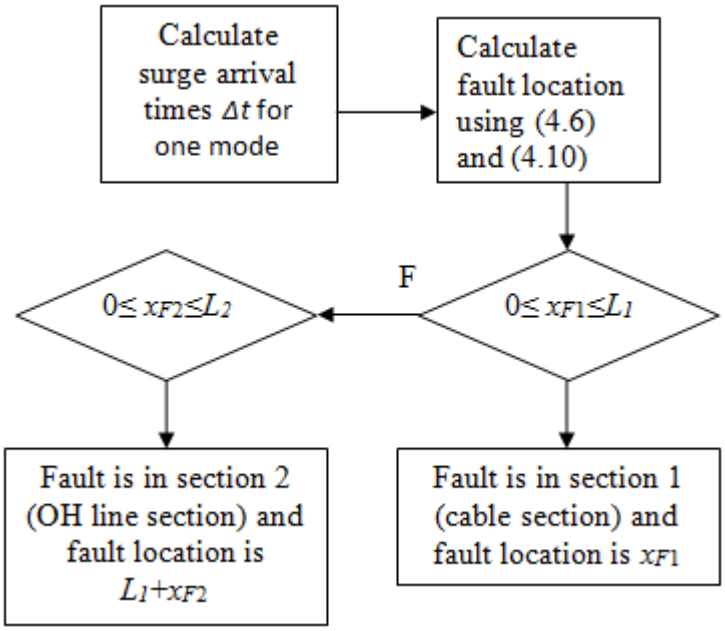

Figure 4.4 Algorithm for the 2-segment hybrid system

Δt can be determined through visual inspection of the Rogowski coil modal voltages, or it can be automated by programming a software that will find the arrival times which can be programmed as follows:

1. Find steady state peak ripple
2. Set a threshold that is at least twice the peak ripple through trial and error
3. Find the times when each terminal Rogowski coil modal voltage reaches the threshold level, then find Δt.

Rogowski coil modal voltages will be explained is section 4.3.1. Choosing a proper threshold level is critical to have accurate results. This will be shown later in chapters 6 and 7.

4.1.3 Hybrid System with Three Sections (Two OH Sections and a Cable)

In this section, the theory and the algorithm for when there are 3 sections are developed as shown in Figure 4.5. The procedure is very similar to the one in the previous section.

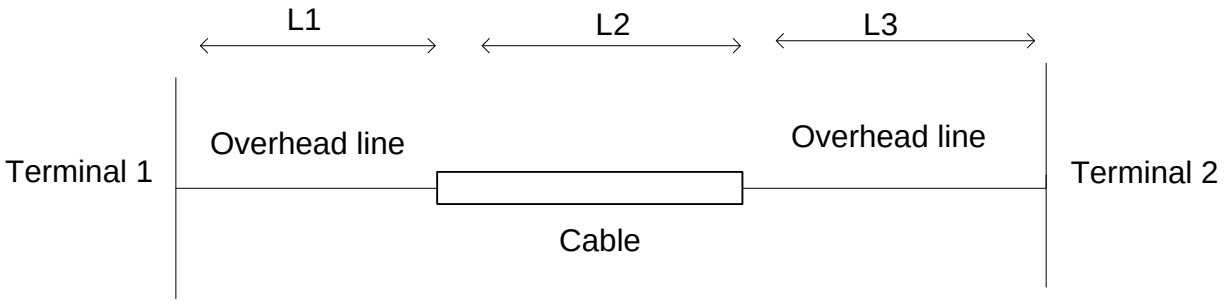

Figure 4.5 Hybrid 3-segment system

First, let us consider, fault case 1, where a fault occurs at the first overhead line section as shown in Figure 4.6.

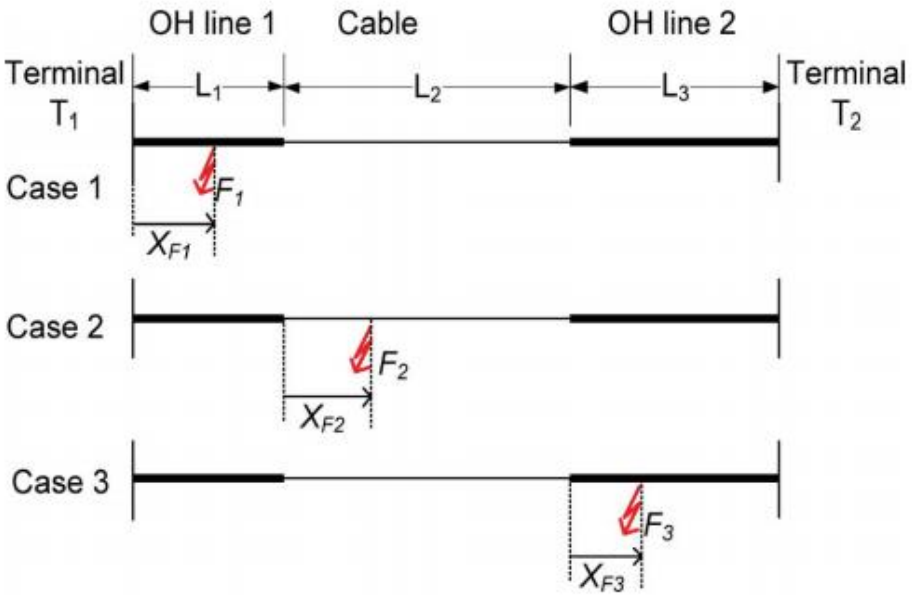

Figure 4.6 Fault scenarios for the three-segment system [6]

The arrival time of traveling wave for F1 at terminal 1 is

$$t_{1-F1} = \frac{x_{F1}}{v_1} \tag{4.11}$$

The arrival time of traveling wave for F1 at terminal 2 is

$$t_{2-F1} = \left(\frac{L_1 - x_{F1}}{v_1}\right) + \frac{L_2}{v_2} + \frac{L_3}{v_3} \tag{4.12}$$

The difference between the arrival times is

$$\Delta t_{12-F1} = t_{1-F1} - t_{2-F1} = \left(\frac{2 \cdot x_{F1}}{v_1} \right) - \frac{L_2}{v_2} - \frac{L_3}{v_3} \tag{4.13}$$

The distance to the fault from the left terminal is

$$x_{F1} = (\Delta t_{12-F1} + \frac{L_1}{v_1} + \frac{L_2}{v_2} + \frac{L_3}{v_3}) \times \frac{v_1}{2} \tag{4.14}$$

Now, let us consider, case 2, where a fault occurs at the middle segment. The equations for the arrival times of the initial traveling waves at terminals 1 and 2, respectively, are

$$t_{1-F2} = \frac{x_{F2}}{v_2} + \frac{L_1}{v_1} \tag{4.15}$$

$$t_{2-F2} = (\frac{L_2 - x_{F2}}{v_2}) + \frac{L_3}{v_3} \tag{4.16}$$

The difference between the arrival times is

$$\Delta t_{12-F2} = t_{1-F2} - t_{2-F2} = \left(\frac{2 \cdot x_{F2}}{v_2} \right) + \frac{L_1}{v_1} - \frac{L_2}{v_2} - \frac{L_3}{v_3} \tag{4.17}$$

Therefore, the fault location from the start of segment 2 from the left is

$$x_{F2} = (\Delta t_{12-F1} - \frac{L_1}{v_1} + \frac{L_2}{v_2} + \frac{L_3}{v_3}) \times \frac{v_2}{2} \tag{4.18}$$

Finally, let us consider case 3, where a fault occurs at the last section. The fault location measured from the beginning of segment 3 from the left can be derived in the same manner as the other fault cases, and it is found to be

$$x_{F3} = (\Delta t_{12-F3} - \frac{L_1}{v_1} - \frac{L_2}{v_2} + \frac{L_3}{v_3}) \times \frac{v_3}{2} \tag{4.19}$$

Where Δt_{12-F3} is the difference between surge arrival times at the two terminals for fault F_3.

In order to find fault location for the 3-section system, the algorithm ,which is developed by [6] is used. The algorithm is shown in Figure 4.7

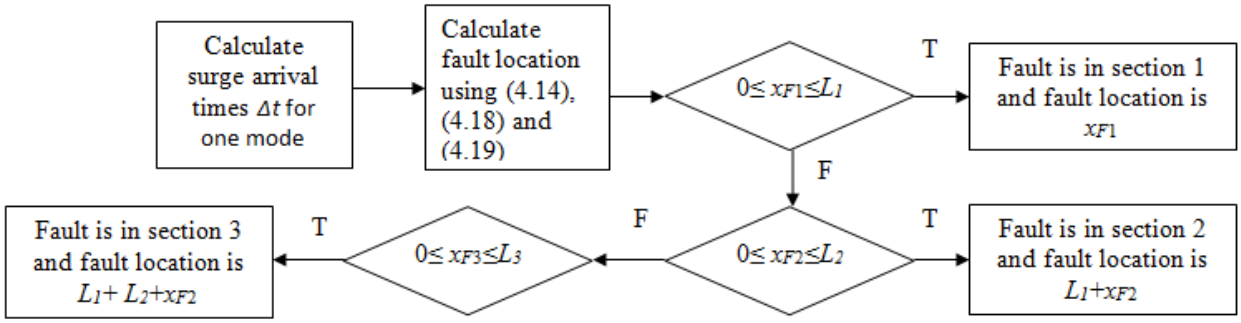

Figure 4.7 Algorithm for the hybrid 3-segment system

Δt can be determined through visual inspection of the Rogowski coil modal voltages, or it can be automated by programming a software as explained in section 4.1.2.

4.2 SURGE ARRIVAL TIME DETECTION METHOD

Rogowski coil will be used here because it proved to be useful in finding the surge arrival times in a VSC-HVDC system and due of its simplicity and other advantages [10]. It also has the ability to measure a wide range of currents from tens of amps to thousands of amps, and it does not saturate [17]. In addition, it gives a voltage output that is proportional to the rate of change of the current, which makes it produce zero output when measuring DC current and non-zero during transients. Usually, an integrator is used in order to determine an output voltage that is proportional to the measured current. However, it is advantageous here not to use an integrator

because the surge arrival times can be found easily through the rate of change of current [10]. Figure 4.8. shows a picture illustrating the Rogowski Coil.

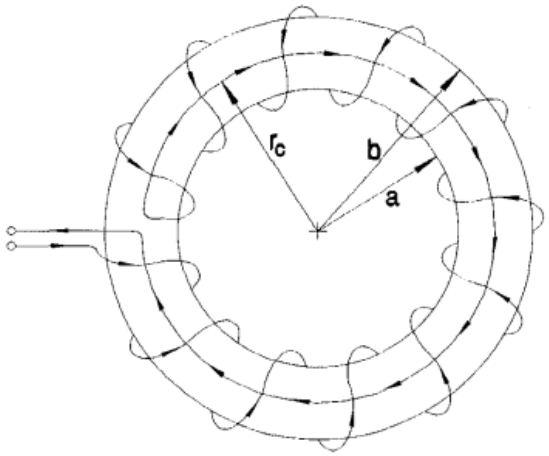

Figure 4.8 Rogowski Coil illustrative draw [17]

When Rogowski Coil placed around a conductor, it produces voltage *e(t)* as in equation (4.20) [14]:

$$e(t) = M \frac{di(t)}{dt} \tag{4.20}$$

Where: $\frac{di(t)}{dt}$ is the rate of change of current in the conductor and *M* is the mutual inductance of the coil. Refer to section 7.1 for more information on why using Rogowski coil voltage output is more beneficial than using current measurements.

4.3 MODAL TRANSFORMATION

Modal domain gives a more accurate representation of current and voltage measurements of multi-phase lines. This is because lines of the multi-phase systems are tightly coupled due to the admittances and the mutual impedances between the lines. The *n* coupled phases of the multi-phase lines are represented by *n* uncoupled propagation modes. The transformation is done by using the modal transformation matrix, which has columns that are Eigen vectors that are associated with parameters of the line. An HVDC system that has two poles, a negative and a positive pole, can be treated like a two-phase system. The voltage and current signals can be transformed into areal and ground mode signals. The modal signals are expected to have better accuracy in terms of calculating fault location because each mode has a distinct propagation velocity. On the other hand, if the signals are used directly without modal transformation, they could lead to errors, because the original signals contain components of both modes while only one propagation velocity is used [10]. The pole to modal transformation of the two-pole HVDC system is shown in equation (4.21) [10]:

$$\begin{bmatrix} V_{mo} \\ V_{m1} \end{bmatrix} = T \cdot \begin{bmatrix} V_P \\ V_N \end{bmatrix} \tag{4.21}$$

Where T is the orthogonal transformation matrix in (4.22)

$$T = \frac{1}{\sqrt{2}} \begin{bmatrix} 1 & 1 \\ 1 & -1 \end{bmatrix} \tag{4.22}$$

And V_P is the voltage measured in the positive pole and V_N is the voltage measured in the negative pole. V_{m0} denotes mode 0 voltage and V_{m1} denotes mode 1 voltage. The current modal transformation is done in the same manner as described by equations (4.21) and (4.22). In general, the transformation matrix is frequency dependent if the line is not ideally transposed.

However, it can be approximated with a small error for other cases, which is what has been done here [10].

4.3.1 Rogowski Coil Voltage Modal Transformation

The Rogowski coil voltage output can be transformed in the same manner as in equations (4.21) and (4.22). This can be proven intuitively be realizing that the scaling and differentiation properties are linear mathematical properties, and the Rogowski voltage output is related by scaling and differentiating the actual current as shown in equation (4.20). For details on the proof see [10].

5.0 PSCAD MODELS

This section shows the models implemented in PSCAD for testing the algorithm.

5.1 TRANSMISSION LINE MODELS

5.1.1 Cable Model

The cable was modeled for a 500 kV HVDC system as in Figure 5.1, Where permittivity was set to 2.5 and the resistance information is found in [19].

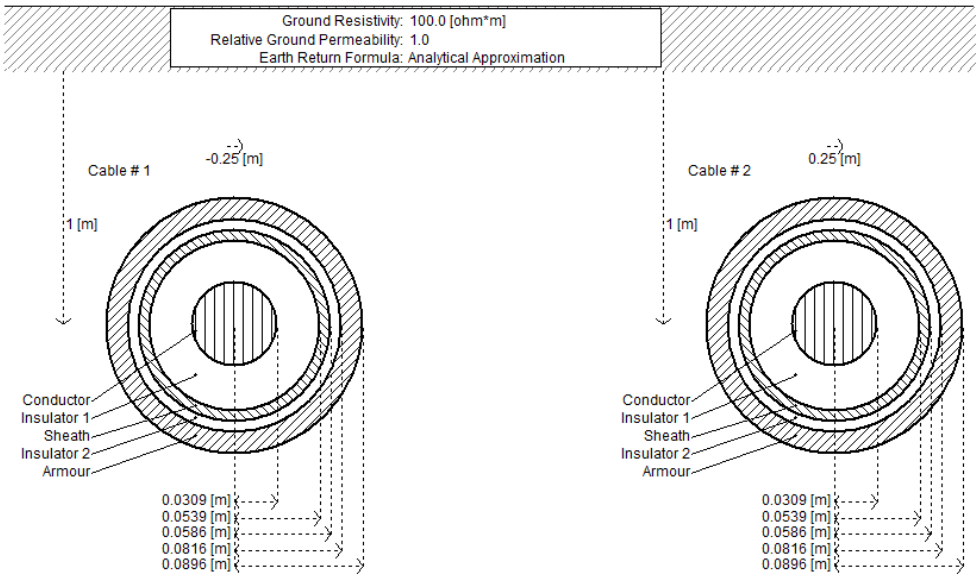

Figure 5.1 Underground cable model based on [18] and [19]

5.1.2 Overhead Line Model

The overhead line is modeled based on [20] as in Figure 5.2. Data for the conductors were obtained from [21]. The conductor data is as follow: Conductor name: Cardinal, GMR= 0.0122834 m, DC resistance=0.06083 ohms/km at 25^{o} C.

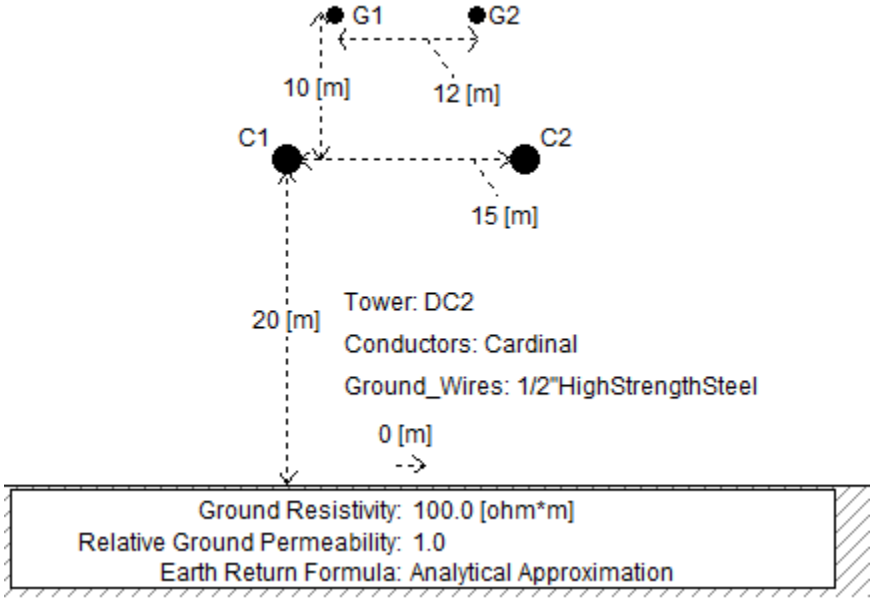

Figure 5.2 Overhead Line Model

5.2 ROGOWSKI COIL MODEL

Rogowski coil was mathematically modeled in PSCAD using a derivative block and a multiplication block as in Figure 5.3. The mutual inductance value was chosen as to magnify damped waves because of faults near terminal units. This is chosen by applying a test fault at 1

km of the system shown in Figure 5.5 and then increasing the value of M that would produce a high enough of a spike for damped signals that could be detected automatically through the algorithm. See the next section for more details.

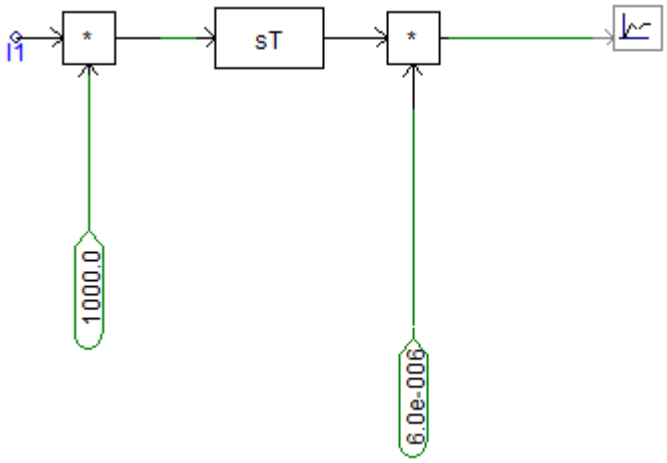

Figure 5.3 Rogowski Coil model in PSCAD

5.3 MODAL TRANSFORMATION

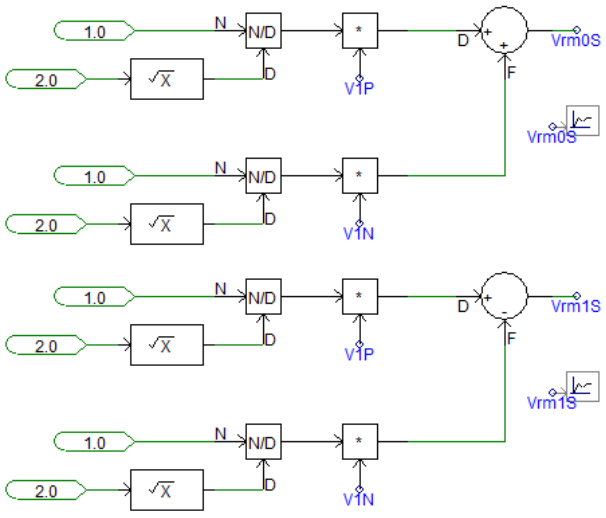

Figure 5.4 Modal transform in PSCAD

5.4 IDEAL DC SOURCE SYSTEM MODEL IN PSCAD

I. Model with Overhead Line

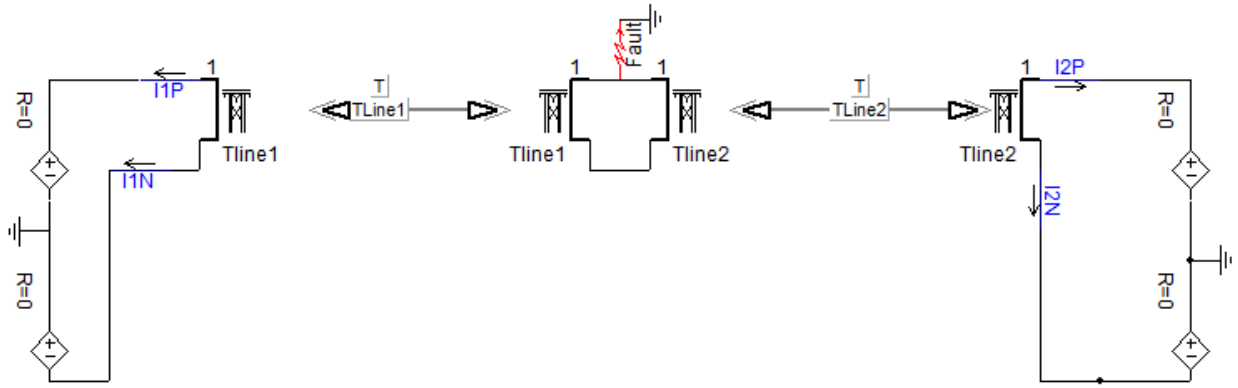

Figure 5.5 Ideal DC source system model with an overhead line

II. Model with Cable

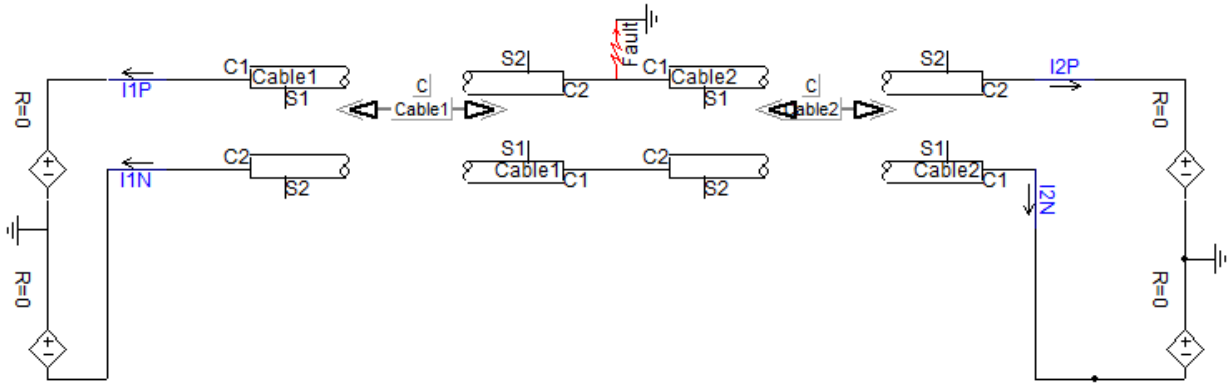

Figure 5.6 Ideal DC source system model with a cable

III. Model with cable and overhead line

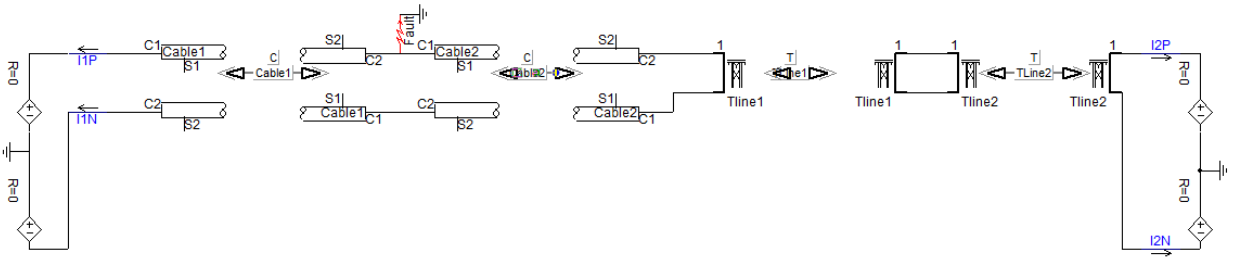

Figure 5.7 A hybrid Ideal DC source system with a cable segment and an overhead line segment

5.5 VOLTAGE SOURCE CONVERTER MODEL

The voltage source converter model used is the one in the PSCAD example projects. The rectifier model is shown below where the power electronic switches are GTOs connected in parallel with a Snubber circuit.

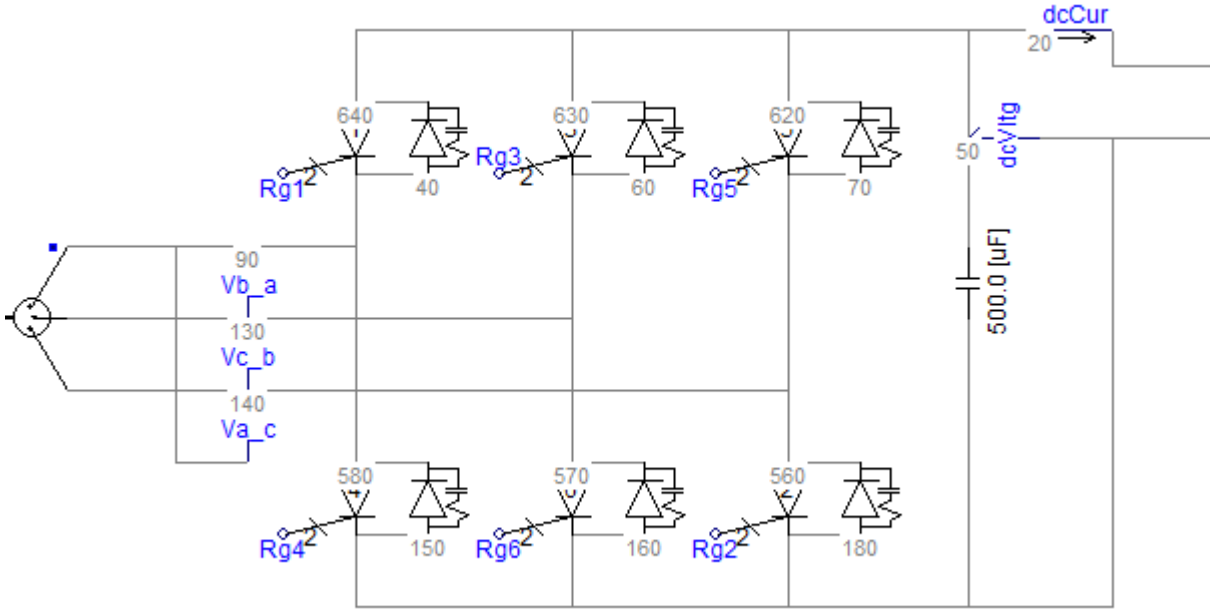

Figure 5.8 PSCAD VSC converter unit model

The inverter model is the same as the rectifier model but connected in the reverse direction. The control teqchique used is PWM. For more information please see the example projects in PSCAD.

6.0 IDEAL DC SOURCE SIMULATION RESULTS AND DISCUSSION

The method was first tested on a system with ideal DC source system and then it was verified with the VSC-HVDC system in chapter 7.

6.1 ONE-SEGMENT SYSTEM RESULTS

6.1.1 Overhead Line Results

The velocity of the wave can be calculated from line geometry. However, the velocity was found experimentally here for better accuracy. It was found by applying a test fault at the sending end terminal of a 600km length overhead line and applying the method in section 4.1.1. Mode 0 velocity was found to be 298424579 m/s and mode 1 velocity was found to be 299956317 m/s. The fault applied here is a P-G fault occurring at t=0.5s for a duration of 0.2s at the positive pole. There is no need to investigate other fault scenarios as the method is theoretically developed for all fault types except for double faults. The fault resistance was set to 0.01 Ω. In [6] and [10], changing the value of the fault resistance did not induce much changes in the results. Therefore, changing the fault resistance will not be investigated here. Table 2 and Table 3 show the results for mode 0 and mode 1, respectively. The parentage error was calculated according to (6.1).

$$Error(\%) = \frac{|Actual\ Fault\ Location - Calculatedd\ Fault\ Location|}{Length\ of\ the\ Line} \times 100 \quad (6.1)$$

The time difference was obtained by visual inspection of the plots in this section. For non-modal results, the error was very large, more than 10km so the results were omitted. Mode 0 had worse results than mode 1. That can be explained in Figure 6.1 and Figure 6.2. For mode 0, the surges were damped too much which makes detecting surge arrival times harder. There are two ways to solve this problem. The first one is to use Wavelet Transform, and the second one is to increase the mutual inductance of the Rogowski coil. For now, the results for the mode 1 are pretty good, so these solutions will not be investigated.

Table 2 Mode 0 fault location results for system with overhead lines only for the ideal DC system

Fault location from sending end (km)	Calculated fault location (km)	Error (km)	Error (%)
450	452.2	2.236	0.373
200	198.2	1.769	0.295
150	147.7	2.291	0.382
100	95.63	4.363	0.727
10	10.56	0.557	0.093
1	2.904	1.904	0.317
.5	1.539	1.039	0.173

Table 3 Mode 1 results for system with overhead lines only for the ideal DC system

Fault location from sending end (km)	Calculated fault location (km)	Error (km)	Error (%)
450	449.9	0.100	0.017
200	199.5	0.500	0.083
150	150.0	0.031	0.005
100	99.04	0.960	0.160
10	9.071	0.929	0.155
1	1.536	0.536	0.089
0.5	0.051	0.449	0.075

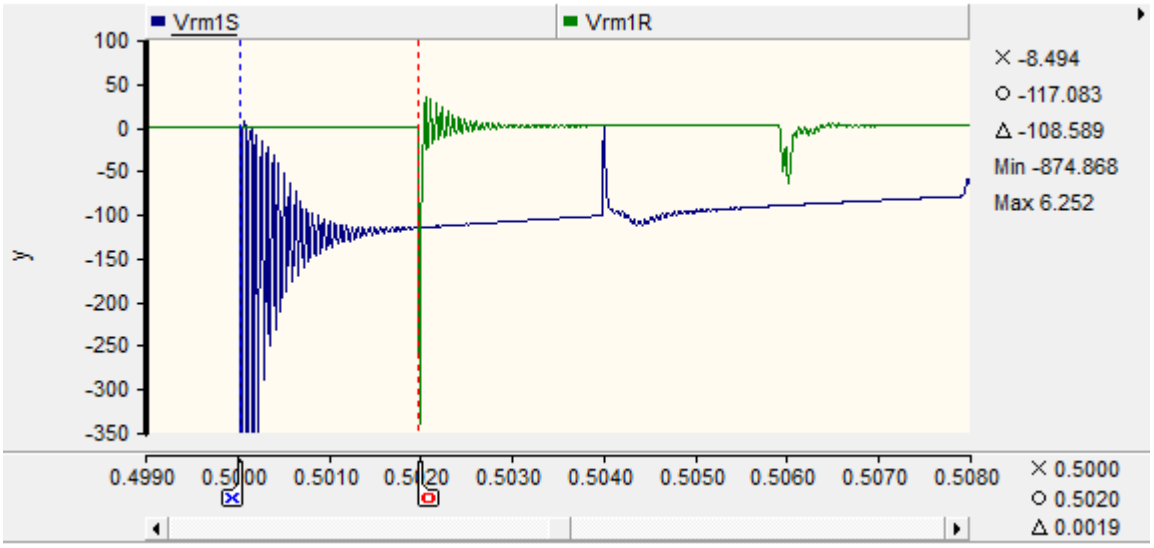

Figure 6.1 Modal voltages of Rogowski coil at both, the receiving end (green) and sending end (blue) for mode 1 results for a fault at 10km from the sending end for the ideal DC system

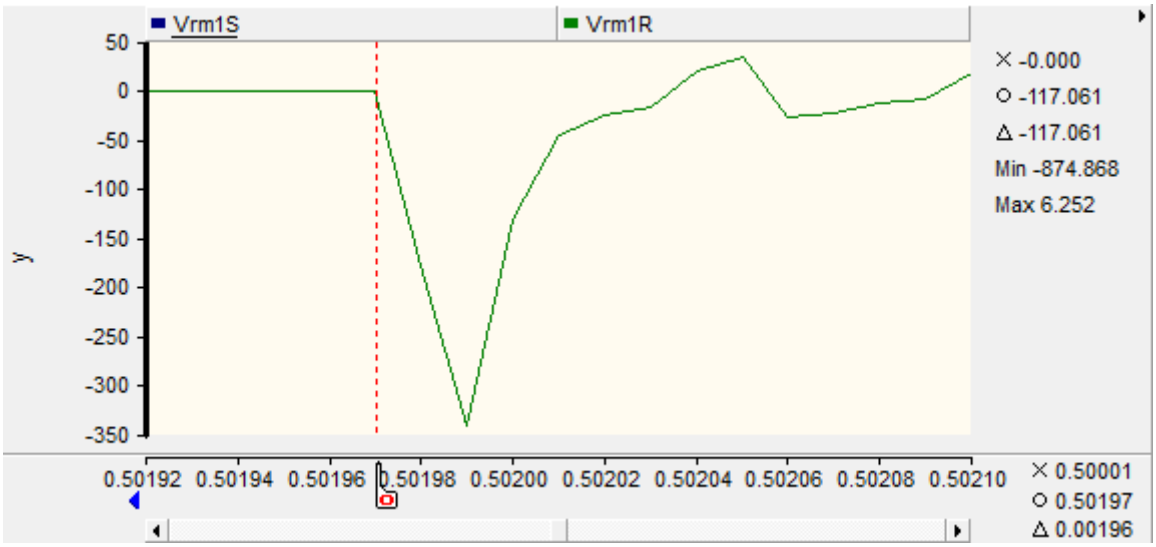

Figure 6.2 The zoomed in receiving end signal for mode 1 for a fault at 10km from the sending end for the ideal DC system

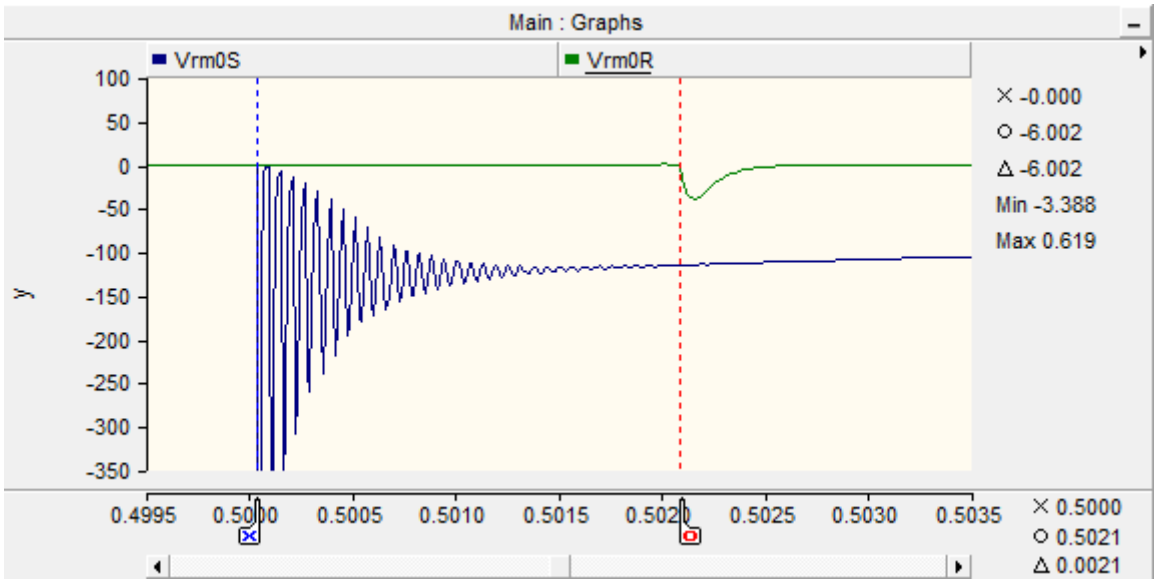

Figure 6.3 Mode 0 results for a fault at 10km from the left showing a low voltage magnitude transient signal which cannot be detected easily for the ideal DC system

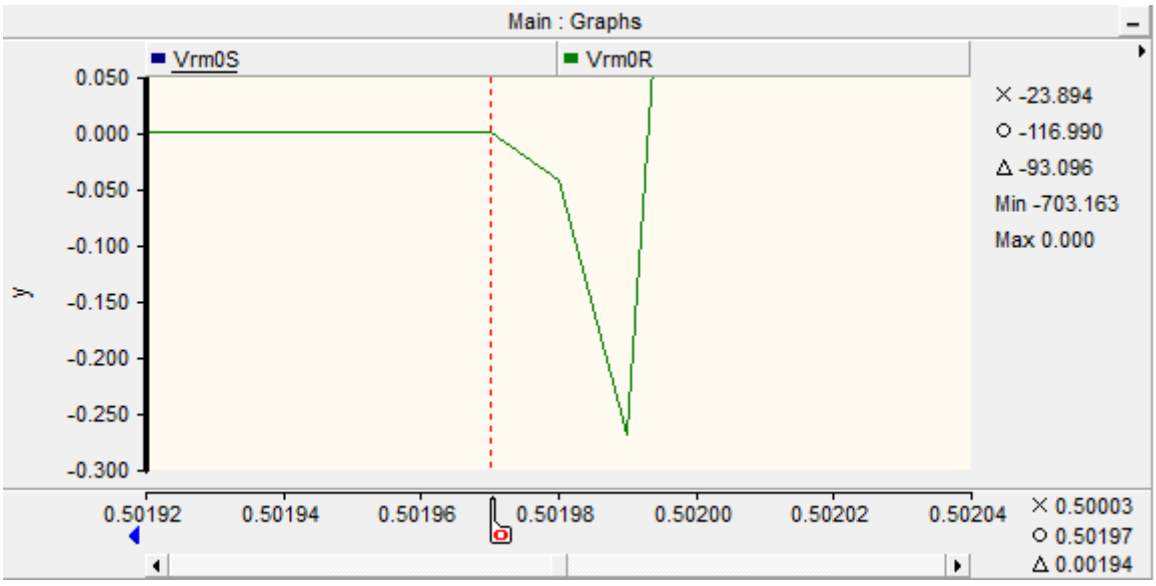

Figure 6.4 Mode 0 results for a fault at 10km from the sending end where the measurement is zoomed in at the receiving end for the ideal DC system

6.1.2 Cable Results

The cable used in this part is a 600km in length. The velocity of the traveling wave in the cable was found by applying a test fault on the sending end of the cable. Mode 0 velocity was found to be 186896103 m/s. Mode 1 velocity was found to be 186907408 m/s. The fault applied here was a P-G fault occurring at t=0.5s at the positive pole for a duration of 0.2s with a resistance of 0.01 Ω. Table 4 and Table 5 show the results for mode 0 and mode 1, respectively, using the method in section 4.1.1. The time difference was obtained by visual inspection of the plots. From Figure 6.6, it can be seen that the surge arrival time can be seen visually when zoomed in. However, it is harder to detect this precise time using the algorithm.

Table 4 Mode 0 results for the ideal DC system with a cable

Fault location from sending end (km)	Calculated fault location (km)	Error (km)	Error (%)
450	451.4	1.394	0.232
200	201.0	1.000	0.167
150	148.7	1.348	0.225
100	100.0	0	0
10	10.31	0.304	0.051
1	0.045	0.954	0.159
0.5	1.858	1.358	0.226

Table 5 Mode 1 results for the ideal DC system with a cable

Fault location from sending end (km)	Calculated fault location (km)	Error (km)	Error (%)
450	451.4	1.388	0.231
200	200.9	0.912	0.152
150	148.6	1.361	0.227
100	100.0	0.036	0.006
10	10.30	0.298	0.050
1	0.045	0.995	0.166
0.5	1.900	1.400	0.234

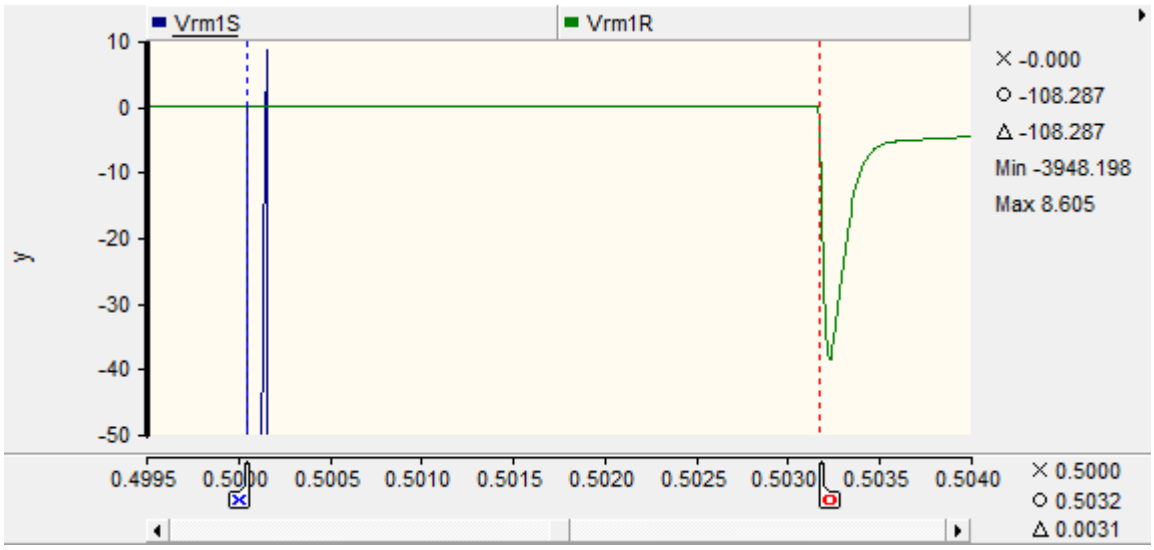

Figure 6.5 Mode 1 results for a fault at 10km from the sending end for the ideal DC system with a cable

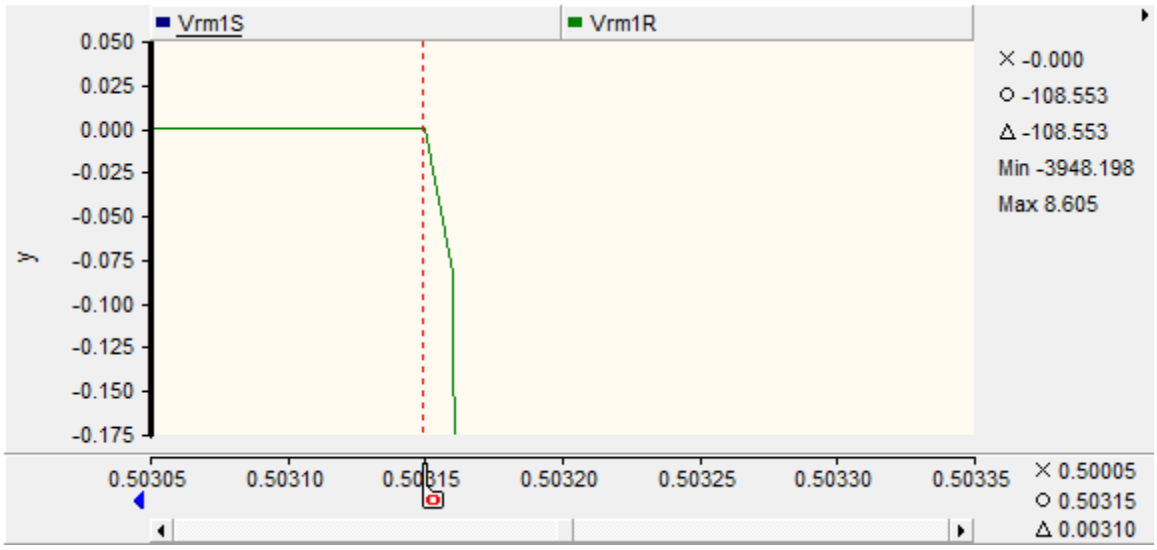

Figure 6.6 Mode 1 results for a fault at 10km from the sending end. The receiving end measurement is zoomed in here for the ideal DC system with a cable

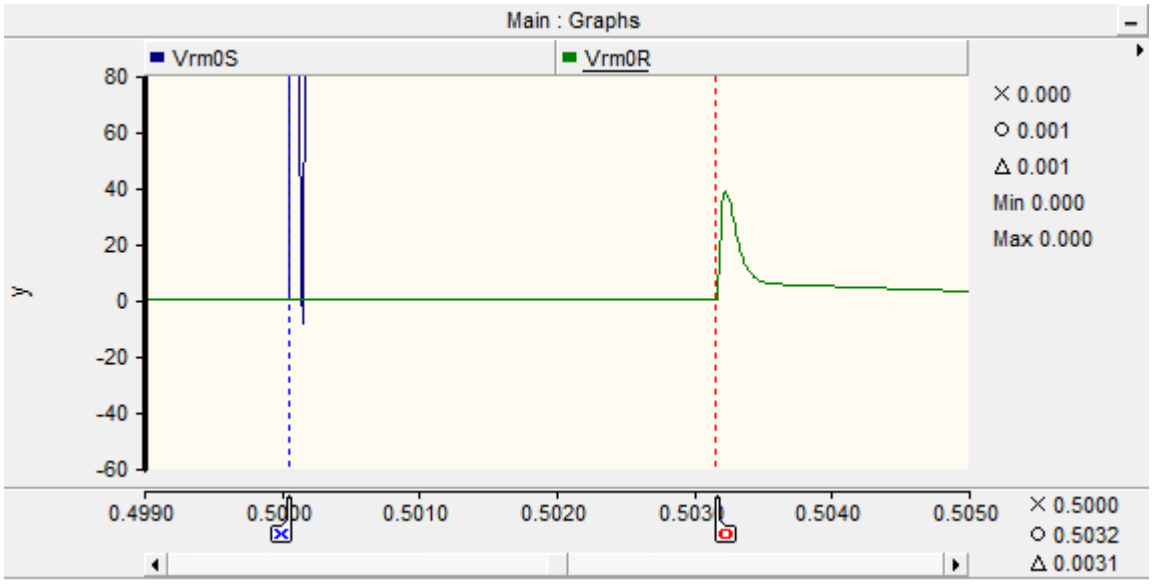

Figure 6.7 Mode 0 results for a fault at 10km from the sending end for the ideal DC system with a cable

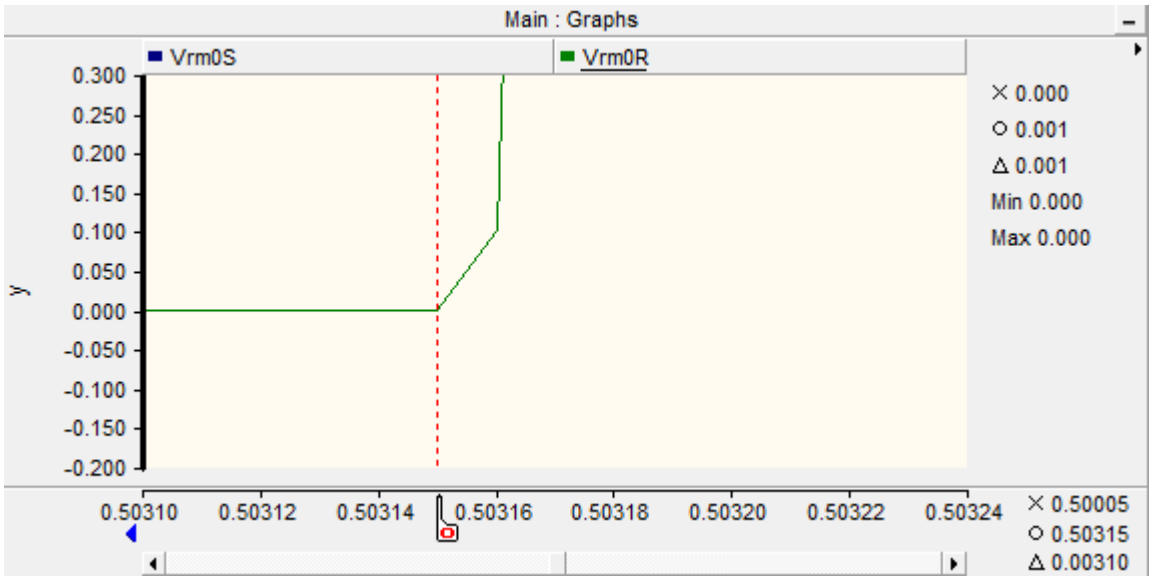

Figure 6.8 Mode 0 results for a fault at 10km from the sending end. The receiving end measurement is zoomed in this graph for the ideal DC system with a cable

6.2 HYBRID (2- SECTION SYSTEM) RESULTS

This section provides the results for the hybrid 2-segement system where the cable length is 300 km and the overhead line length is 300 km as well. The fault applied here was a P-G fault occurring at t=0.5s at the positive pole for a duration of 0.2s with a resistance of 0.01 Ω. For the cable, mode 0 velocity was found to be 189815099 m/s and mode 1 velocity was found to be 189826760 m/s. For the overhead line, mode 0 velocity was found to be 303134350.3 m/s and mode 1 velocity was found to be 303112048.5 m/s. The threshold was set to 0.005 kV for both modes. Table 6 shows the results for mode 0 and Table 7 shows the results for mode1 using the method in section 4.1.2.

Table 6 Results for mode 0 signal for the hybrid 2-segment ideal DC system

Fault location from sending end (km)	Calculated fault location (km)	Error (km)	Error (%)
150	147.1	2.879	0.480
200	198.4	1.629	0.272
300	298.0	1.976	0.329
350	348.4	1.624	0.271
400	399.9	0.091	0.015
450	451.4	1.442	0.240
599	Can't be determined	N/A	N/A

For a fault at 599 km, the fault location cannot be determined using mode 0 and a 0.005 volts Threshold. When the threshold is decreased to 0.000005 volts, the fault location was found to be 599.9.

Table 7 Results for mode 1 signal for the hybrid 2-segment ideal DC system

Fault location from sending end (km)	Calculated fault location (km)	Error (km)	Error (%)
150	149.0	0.974	0.162
200	200.3	0.279	0.046
300	299.0	1.011	0.168
350	348.4	1.601	0.267
400	398.4	1.588	0.265
450	449.9	0.059	0.010
599	599.9	0.982	0.164

For the mode 1 signal, the fault at 599km was estimated without the need to change the threshold. Better accuracy could possibly be obtained by changing the threshold level and by measuring velocities that are more precise. This will be attempted later for the VSC-HVDC system as the purpose of this section is just to show that the method works with a reasonable error.

6.3 HYBRID (3-SECTION SYSTEM) RESULTS

Results for the 3-segement system using the method in section 4.1.3 is shown in Table 8 and Table 9 for modes 0 and 1, respectively. Again, the fault applied here was a P-G fault occurring at t=0.5s at the positive pole for a duration of 0.2s with a resistance of 0.01 Ω . The system consists of two 300 km overhead line segments and one 300 km cable segment in the middle. The speeds were calculated again for better accuracy and they were found to be v_1=300000000 m/s for the overhead line, and v_2=189000000 m/s for the cable. These speeds were used for both modes. The threshold was set to be 0.005 Volts through calibration by conducting different experiments.

Table 8 Results for mode 0 signal for the hybrid 3-segment ideal DC system (error >1%)

Fault location from sending end (km)	Calculated fault location (km)	Error (km)	Error (%)
50	49.09	0.905	0.100
150	151.1	1.095	0.122
300	301.6	1.635	0.182
350	351.7	1.720	0.191
400	401.8	1.805	0.201
450	452.8	2.835	0.315
650	657.4	7.405	0.823
600	606.4	6.405	0.711
750	759.4	9.405	1.045
899	913.9	14.90	1.656

Mode 0 results gave a very large error value that is too large due to the speed of wave accuracy, surge detection accuracy, and threshold tuning.

Table 9 Results for mode 1 signal for the hybrid 3-segment ideal DC system (error<0.2%)

Fault location from sending end (km)	Calculated fault location (km)	Error (km)	Error (%)
50	49.09	0.905	0.100
150	151.1	1.095	0.122
300	300.7	0.690	0.077
350	350.8	0.775	0.086
400	399.9	0.085	0.009
450	450.9	0.945	0.105
650	649.9	0.095	0.011
600	600.4	0.405	0.045
750	748.9	1.095	0.122
899	898.9	0.095	0.011

Mode 1 showed much better results and the maximum error was 0.122%. This is very reasonable and therefore we will not do any further calibration. The error percentage found here is lower than error percentage obtained in [6] for the Line-Commutated Converter that used Wavelet Transform for edge detection and CT as a measuring device for current measurements.

7.0 HYBRID VSC SIMULATION RESULTS AND DISCUSSION

This chapter shows the simulation results and discusses it for the hybrid case VSC-HVDC systems only.

7.1 HYBRID VSC-HVDC (2-SEGMENT) SYSTEM

In this section, the fault location algorithm is applied for the hybrid 2-segment VSC-HVDC transmission system shown in Figure 1.1 . Before applying the algorithm in section 4.1.2, Rogowski coil mutual inductance needs to be set in order for the worst case traveling wave surge to be detected. Also, a proper threshold needs to be set. To do the first task, a fault is applied at the sending end terminal at t=0.8s for duration of 0.2s and the Rogowski coil modal voltage output at the receiving end is observed. The reason for applying the fault at t=0.8s is to allow a sufficient time for the system to reach steady state. The fault applied here was a P-G fault occurring at the positive pole with a resistance of 0.01 Ω. Figure 7.1 shows the plot for this scenario.

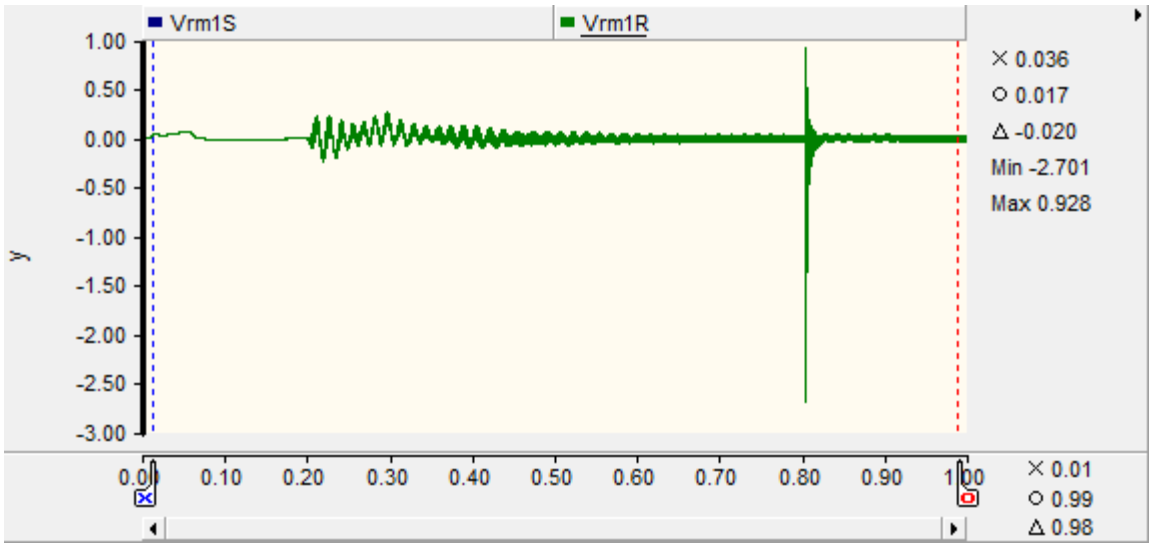

Figure 7.1 Rogowski coil mode 1 voltage at the receiving end for a fault occurring at the sending end for the hybrid (2-segment) VSC-HVDC system

It can be seen from Figure 7.1 that the fault is clearly distinguishable. The fault disturbance is zoomed in in order to see the characteristics more clearly. Figure 7.2 shows the same fault zoomed in.

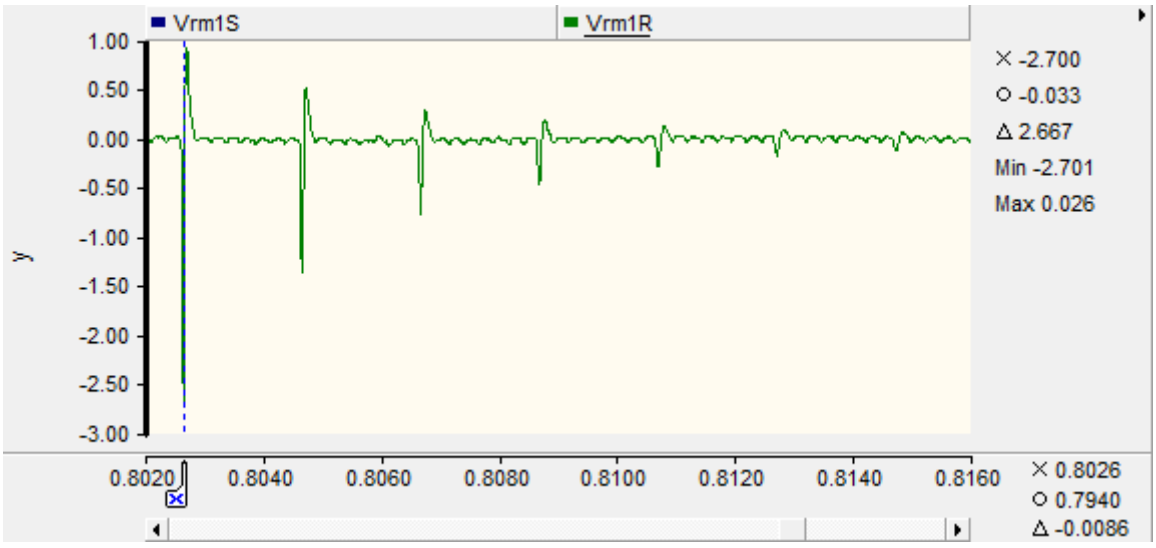

Figure 7.2 The zoomed in Rogowski coil mode 1 voltage at the receiving end for a fault occurring at the sending end for the hybrid (2-segment) VSC-HVDC system

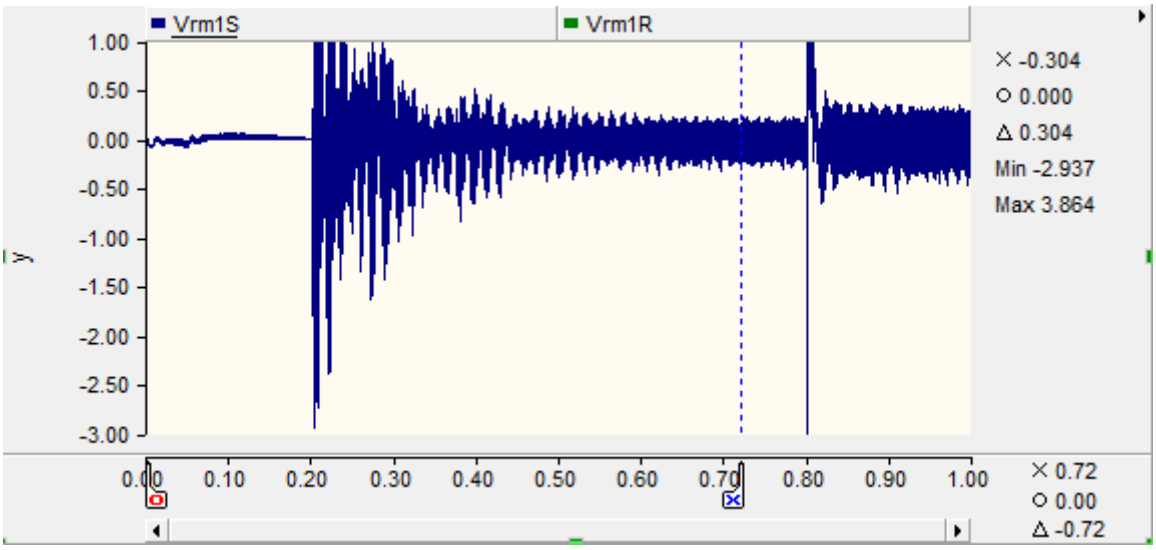

Figure 7.3 Rogowski coil mode 1 voltage at the sending end for a fault occurring at the sending end for the hybrid (2-segment) VSC-HVDC system

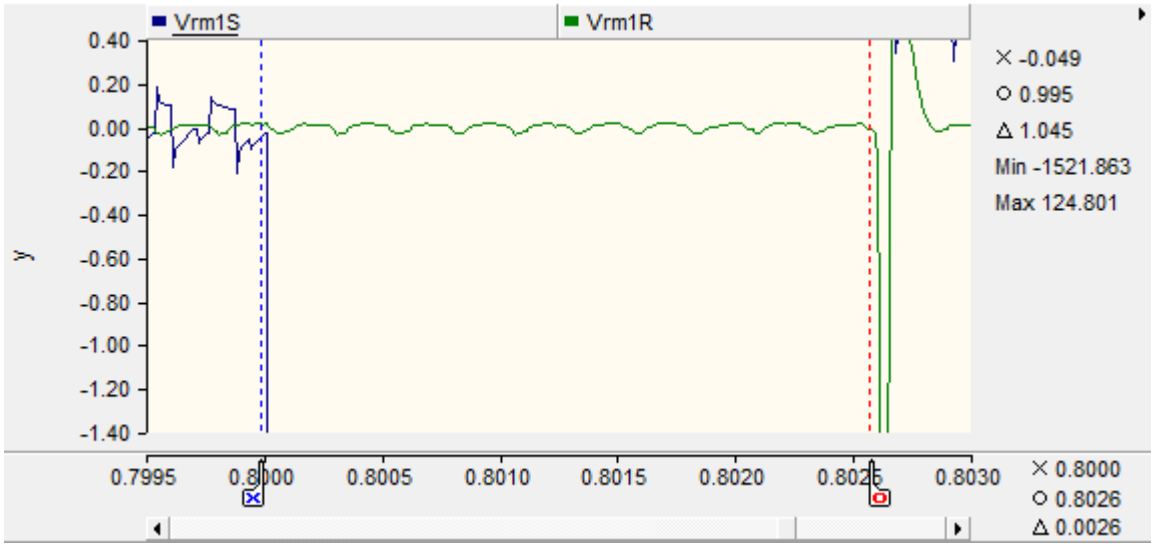

Figure 7.4 Both the receiving end and sending end initial surges showing the time difference for a fault at the sending end for the hybrid (2segment) VSC-HVDC system

From Figure 7.2, we can see that the first traveling wave surge of the Rogowski coil modal voltage is clearly distinguishable and it is has a magnitude of 2.7 volts which is much greater than the receiving end ripple which is 0.033 volts and much greater the sending end

ripple which is 0.304 volts as shown in Figure 7.3. Therefore, there is no need to change the Rogowski coil mutual inductance of 6uH . Also, 2nd, 3rd , 4th and 5th reflections of the fault traveling waves can also be observed clearly in Figure 7.2. This could make one terminal fault location methods possible with complex computations and using signature analysis. Figure 7.4 shows the time differnece needed to calculate fault location using the two terminals. The earlier we can detect the intial fault surges, the more accurate our results are. In addition, Figure 7.1 and Figure 7.2 serve as a validation that the Rogowski coil modal voltages are more useful than just using the current measurements shown in Figure 7.5 and Figure 7.6. This is due to the attenuation of the current surge that is caused by the impedance of the line.

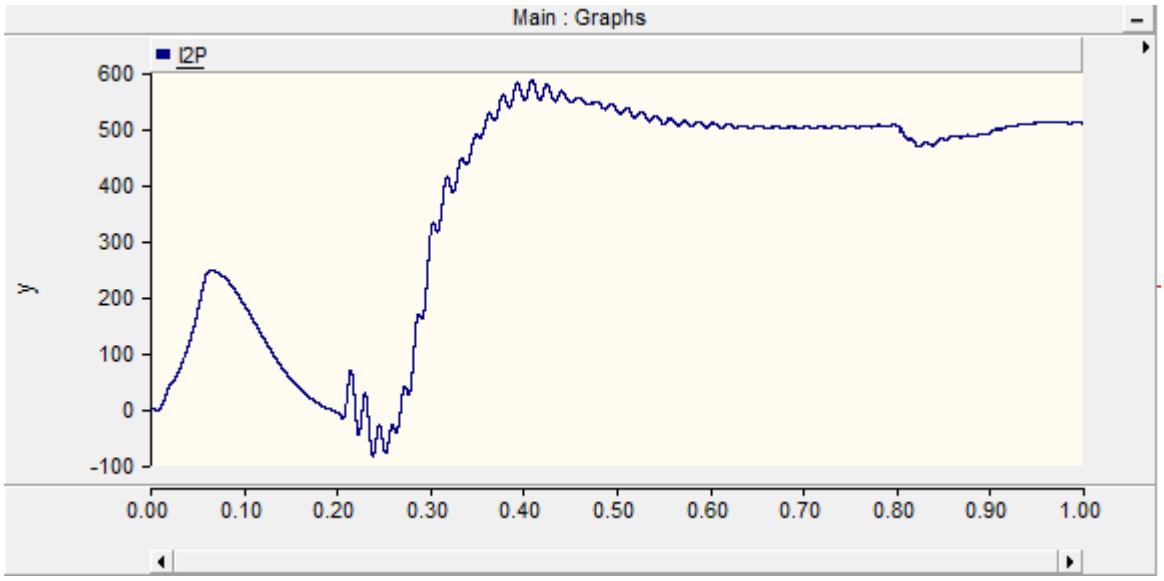

Figure 7.5 Positive pole current measurement at the receiving end for a fault occurring at the sending end for the hybrid (2-segment) VSC-HVDC system

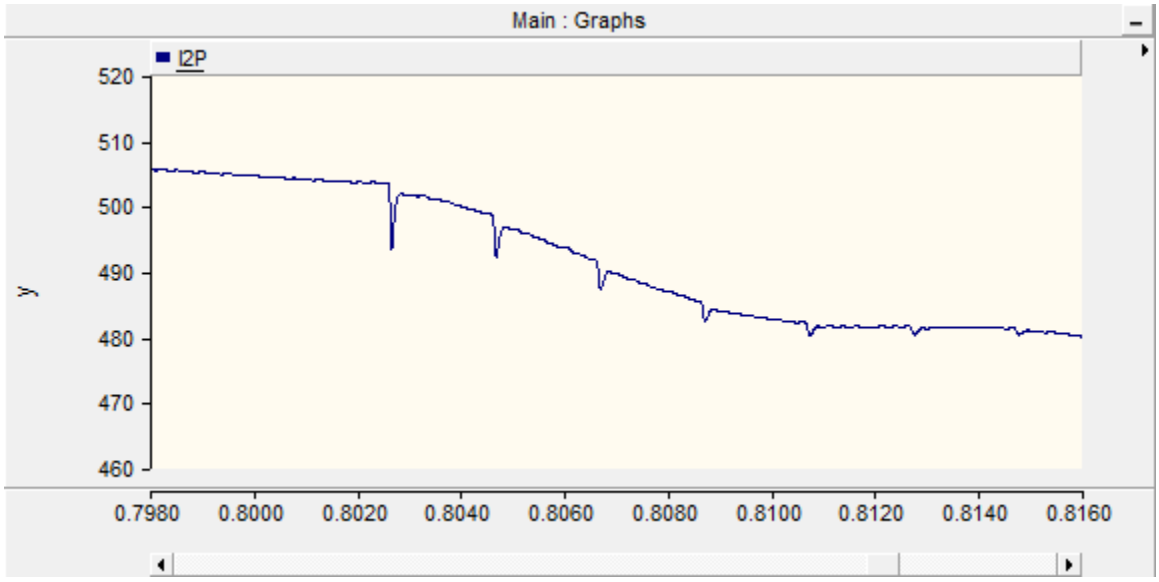

Figure 7.6 Zoomed in positive pole current measurement at the receiving end for a fault occurring at the sending end for the hybrid (2-segment) VSC-HVDC system.

In Figure 7.6, the first 3 reflections can be seen visually when zoomed in at the known fault transient period. However, we claimed earlier that the current measurement is not as useful as Rogowski coil modal voltages. This can be explained by Figure 7.7. In Figure 7.7, the cursers X and O, point at the current fault surge peak and the steady state current ripple peak, respectively. It can be seen that these were, 494.235 A, and 499.898 A, respectively. This is a very small difference, which makes distinguishing the surge from the ripple very hard especially for a system that has larger noise levels and longer lines. This makes it necessary to use edge detection tools such as wavelet transform as has been used in [6] or using Rogowski Coil.

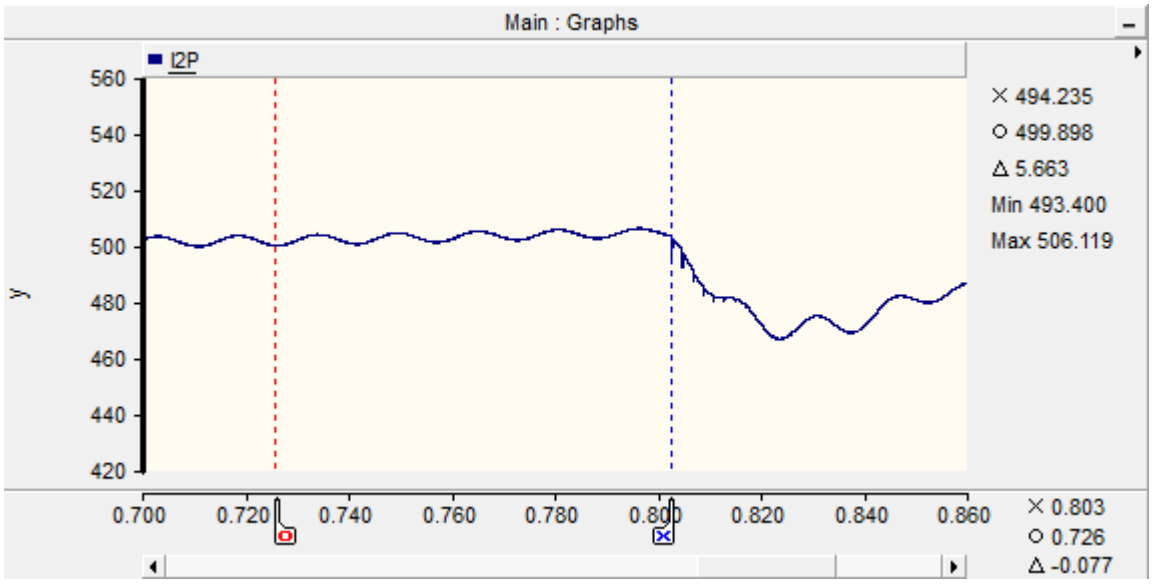

Figure 7.7 Positive pole current measurement at the receiving end showing fault surge peak (cursor X) and noise peak (cursor O) for a fault occurring at the sending end for the hybrid (2-segment) VSC-HVDC system.

In order to set a proper threshold level to be used in the algorithm developed in section 4.1.2, the worst case ripple has to be found. This is done by investigating the steady state signal at the sending end and at the receiving end. The largest ripple magnitude was found to be 0.304 volts. Therefore, the threshold is set to at least 1.5 times larger than the ripple to avoid false detection. Also, the threshold should not be set too large in order to have more accurate results. Here, the threshold is set to twice the ripple which is equal to 0.608 volts. Only mode 1 will be considered here since mode 0 had poorer results than mode 1, which was shown previously in section 6.2. Also, it can be seen clearly in Figure 7.8 and Figure 7.9, that mode 0 results are harder to obtain than mode 1 because the signal is too small.

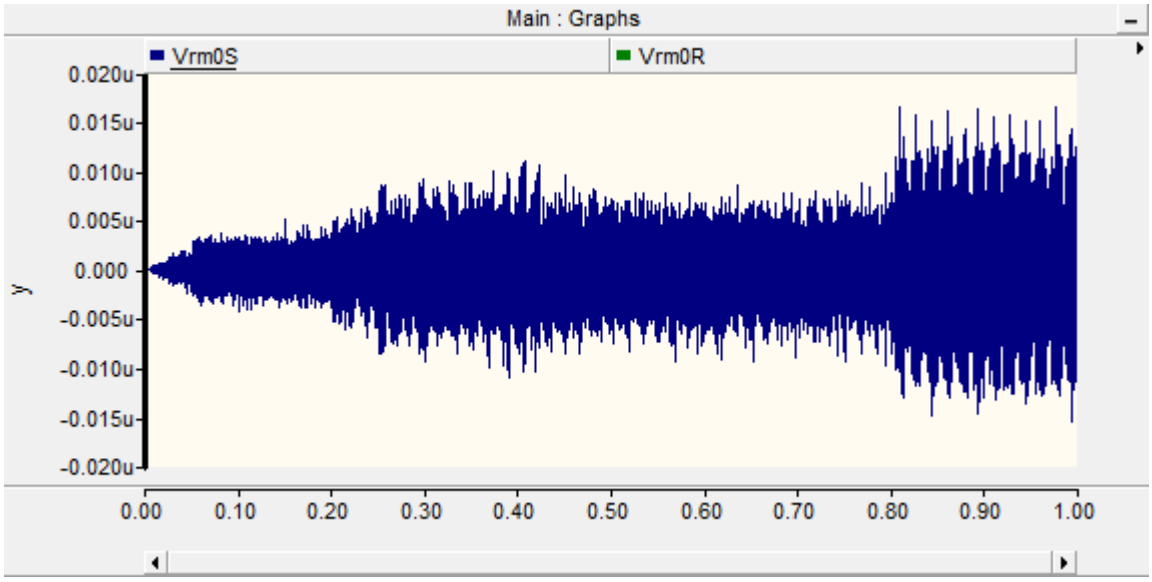

Figure 7.8 Mode 0 sending end signal for a fault at the sending end for the hybrid (2-segment) VSC-HVDC system

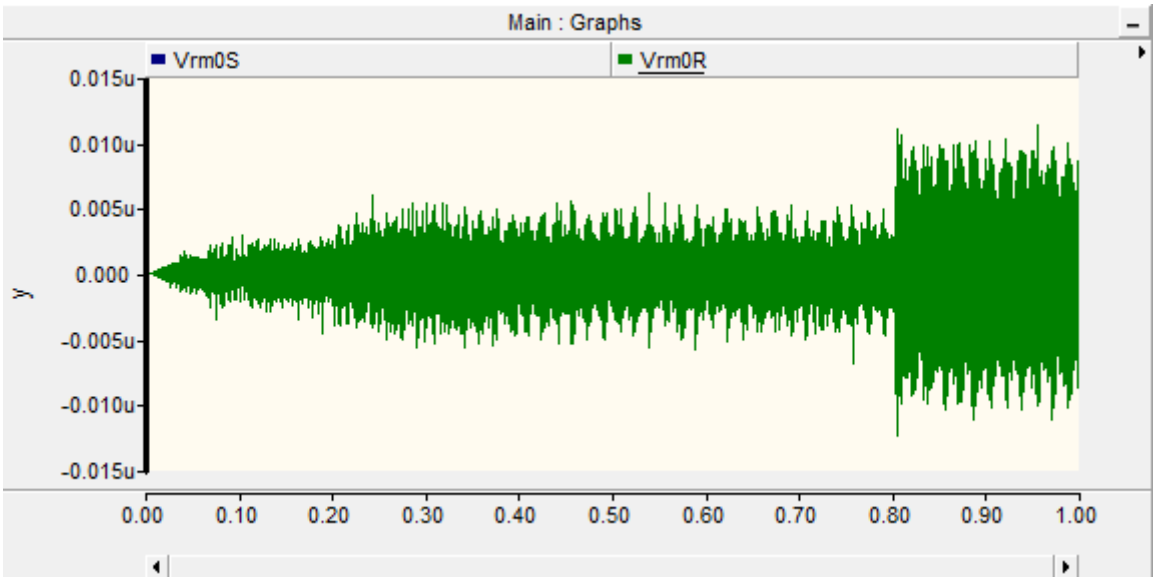

Figure 7.9 Mode 0 receiving end signal for a fault at the sending end for the hybrid (2-segment) VSC-HVDC system.

The speeds of the wave were calculated again by applying a test fault for better accuracy and it is found to be v_1=300000000 m/s for the overhead line and v_2=187200000 m/s for the cable. Table 10 shows the result for this section. The maximum error is 0.23% which shows that the method works pretty well.

Table 10 Fault location results for the hybrid (2-segment) VSC-HVDC system using mode 1 signal

Fault location from sending end (km)	Calculated fault location (km)	Error (km)	Error (%)
150	150.000	0	0
200	199.608	0.3920	0.0653
300	301.115	1.1150	0.1858
350	349.115	0.8846	0.1474
400	398.615	1.3846	0.2308
450	449.615	0.3846	0.0641
599	599.615	0.6154	0.1026

7.2 HYBRID VSC-HVDC (3-SEGMENT) SYSTEM

In this section, the algorithm developed for the hybrid 3-segment system is applied on a VSC-HVDC system which consists of, OH line, Cable, and OH line as shown in Figure 1.2. Before applying the method developed in section 4.1.3, a threshold needs to be set in order to detect the traveling surge due to the worst-case fault. Also, Rogowski coil mutual inductance needs to be set appropriately in order to detect worst case traveling wave faults. A Fault is applied at the sending end terminal at t= 0.8s for a duration of 0.2s, and the voltage is observed at the receiving end in order to determine whether the mutual inductance of the coil is sufficient. Also, the same scenario is used to find out the maximum value of ripple that would be needed in order to set up a proper threshold. Figure 7.10 shows mode 1 Rogowski coil voltage output at the receiving end. From Figure 7.10, it can be clearly seen that the fault is clearly distinguishable from the ripple. The peak steady-state ripple for mode 1 receiving end signal was found from Figure 7.11 to be 0.058 volts

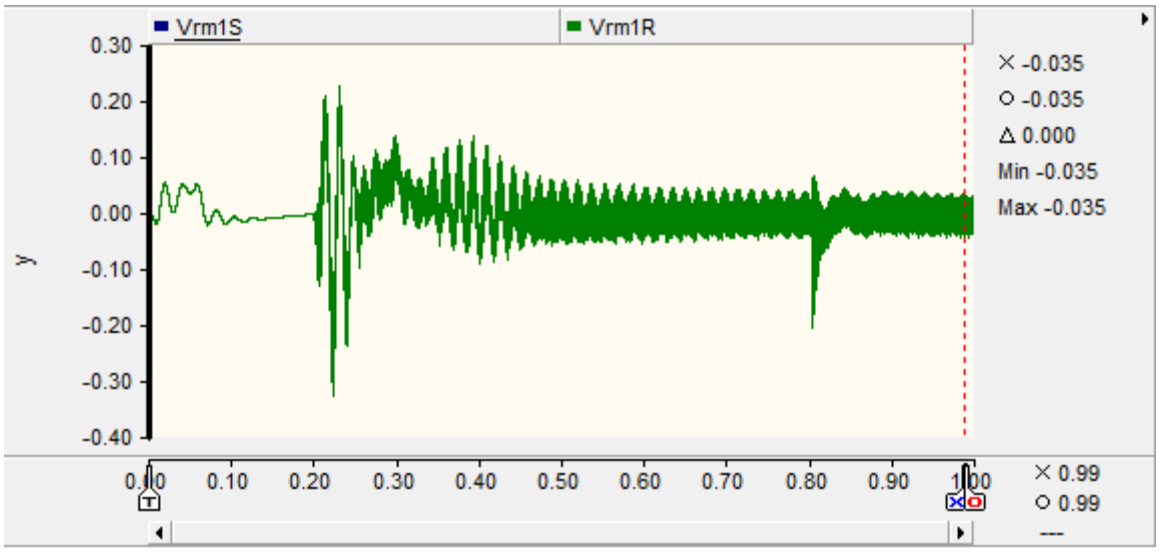

Figure 7.10 Mode 1 receiving end signal for a fault at the sending end for the hybrid (3-segment) VSC-HVDC system

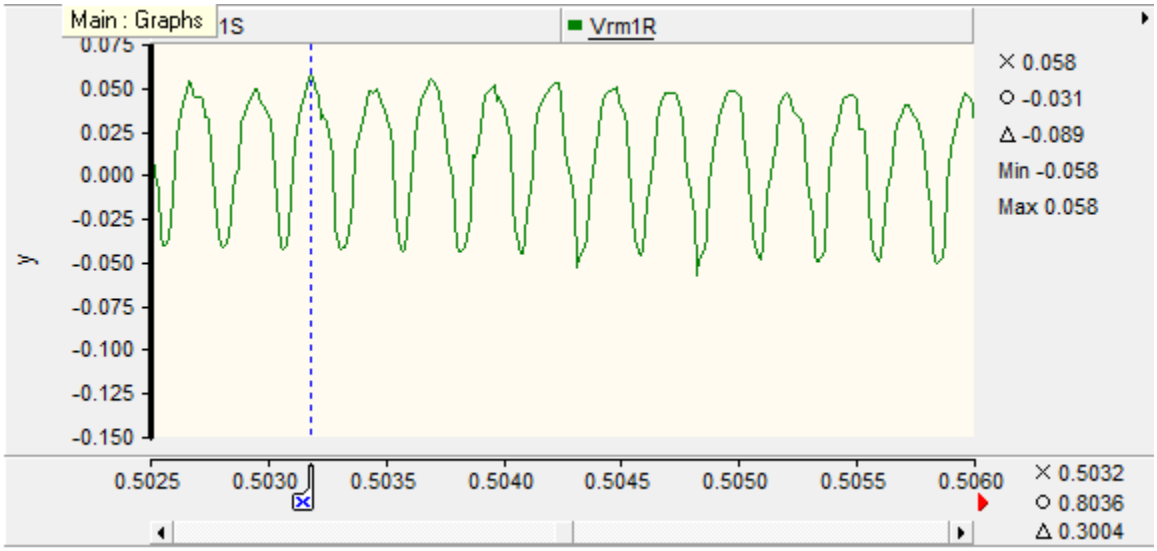

Figure 7.11 Mode 1 receiving end signal zoomed in to show the steady-state ripple for the hybrid (3-segment) VSC-HVDC system.

Now, the fault surge needs to be inspected in order to compare the peak of the first traveling wave surge to the peak ripple. Therefore, the receiving end mode 1 fault surge is zoomed in as shown in Figure 7.12. It can be seen from Figure 7.12 that the the fault surge peak is more than twice the ripple magnitude. Therefore, initially there is no need to change the

Rogowski coil mututal impedance of 6uH. However, the sending end signal is anlayzed in order to complete the calibration process and to double check that the that Rogowski coil mutual inductance value is sufficient . Figure 7.13 shows the sending end mode 1 signal for a fault occuring at the sending end.

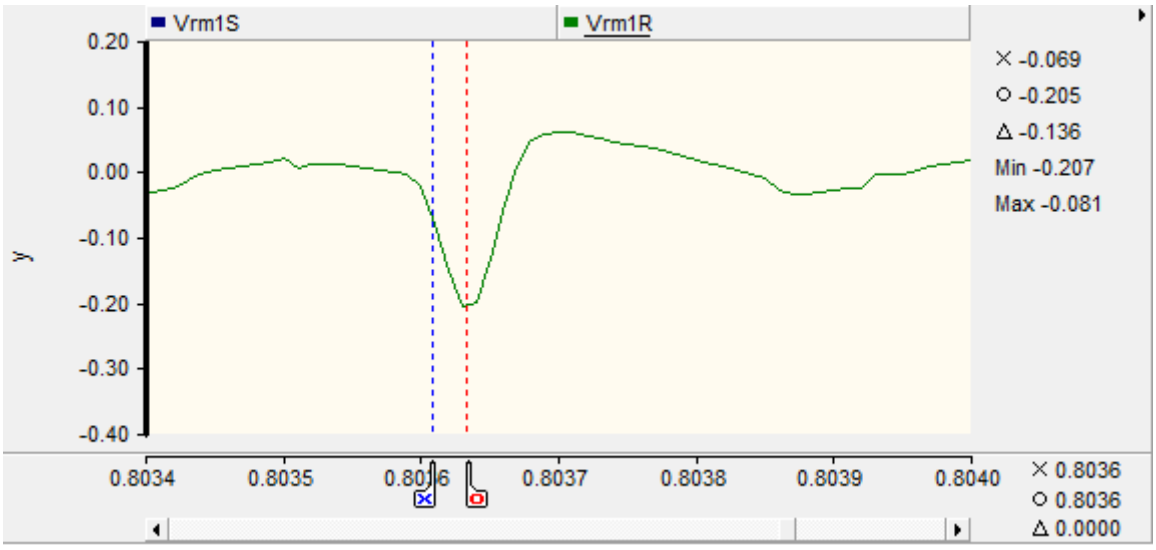

Figure 7.12 Mode 1 zoomed in fault surge appearing at the receiving end for a fault occurring at the sending end for the hybrid (3-segment) VSC-HVDC system

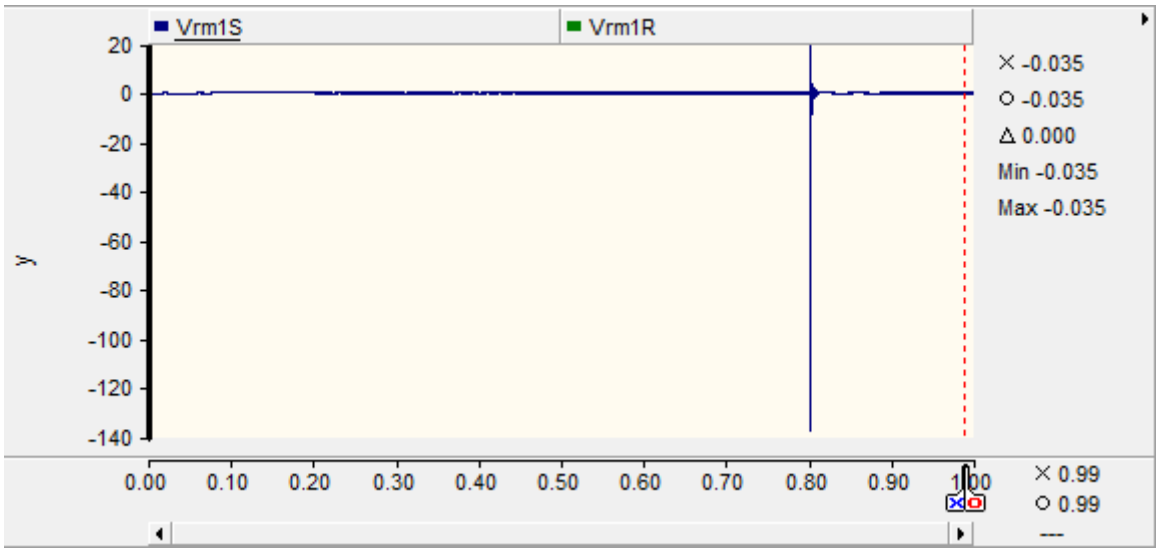

Figure 7.13 Mode 1 fault surge appearing at the sending end for a fault occurring at the sending end for the hybrid (3-segment) VSC-HVDC system

In order to find the peak ripple magnitude, the steady-state part of the sending end measurement is zoomed in as shown in Figure 7.14.

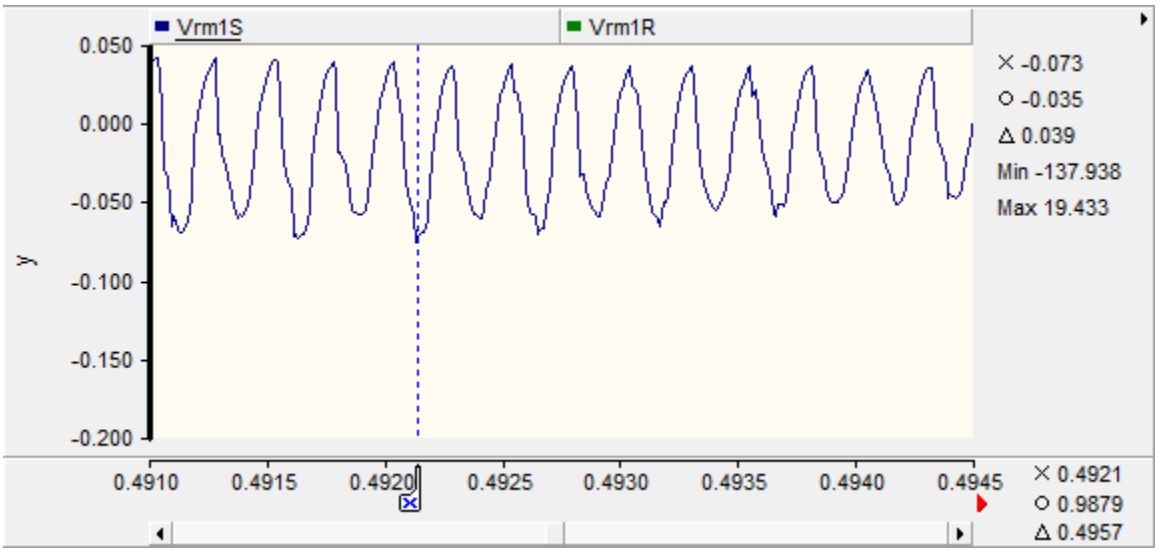

Figure 7.14 The zoomed in Mode 1 steady state signal appearing at the sending to find peak ripple for the hybrid (3-segment) VSC-HVDC system

The maximum ripple magnitude at steady state appears to be equal to 0.073 which is higher than the ripple at the receiving end. The fault surge peak is still more than twice larger than the highest peak ripple magnitude. Therefore, the Rogowski coil mutual inductance value is sufficient. Finally, the threshold is set to 1.5 times the highest peak ripple magnitude. In this case, the threshold is set equal to 0.1095.

Now, we investigate the mode 0 signal and see if it is applicable in finding the fault location. Figure 7.15 and Figure 7.16, show the receiving end and sending end signals for a fault at the sending end, respectively. From these figures, it can be seen that the fault surge is too small and it is not clearly distinguishable from the ripple making it hard to find the arrival times. Therefore, the Rogowski coil mutual inductance is increased to 50 uH for mode 0 in an attempt to make the fault surge more distinguishable. Figure 7.17 and Figure 7.18, show the receiving end and sending end signals, respectively, for this modification for the same fault.

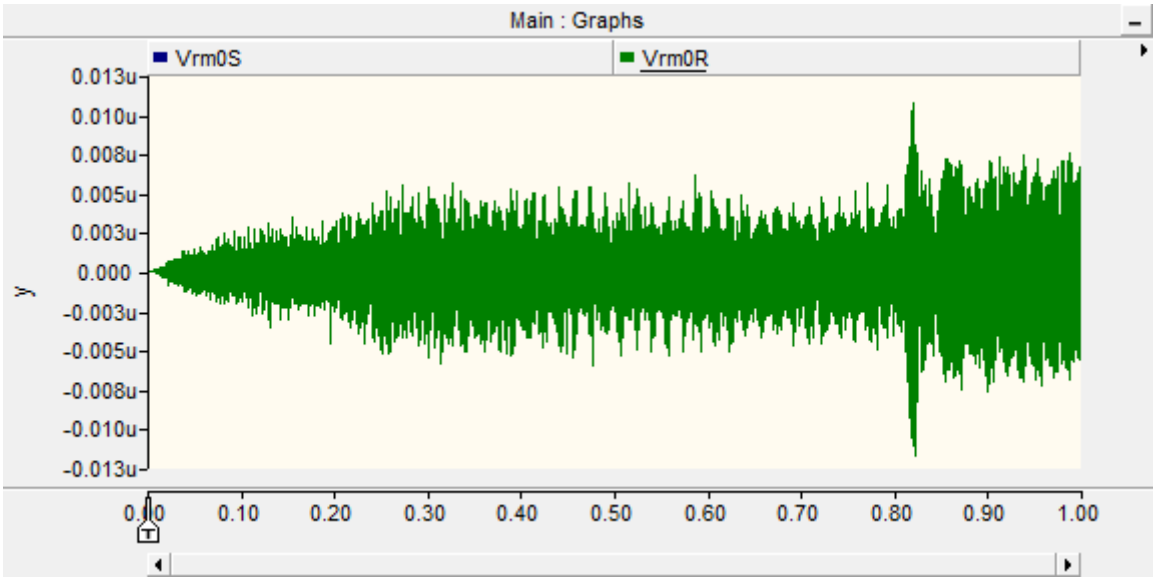

Figure 7.15 Mode 0 receiving end signal for a fault at the sending end for the hybrid (3-segment) VSC-HVDC system

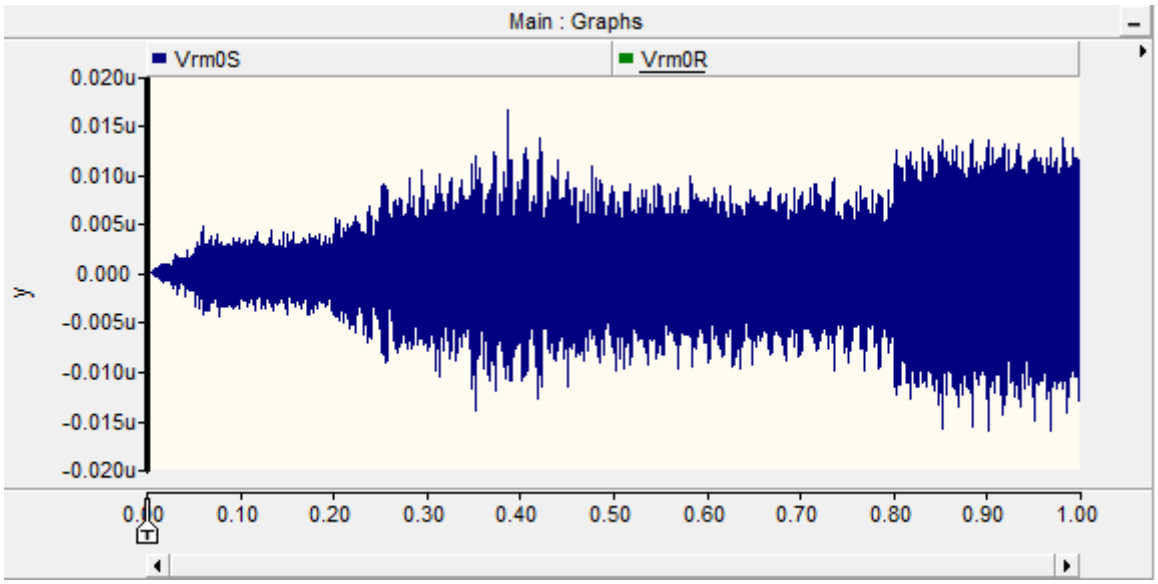

Figure 7.16 Mode 0 sending end signal for a fault at the sending end for the hybrid (3-segment) VSC-HVDC system

From Figure 7.17 and Figure 7.18 below, it still can be seen that the mode 0 signal still does not have a distinguishable fault surge, especially at the sending end, although the Rogowski coil inductance value was changed to a large value. Therefore, only mode 1 would be used to identify the fault location.

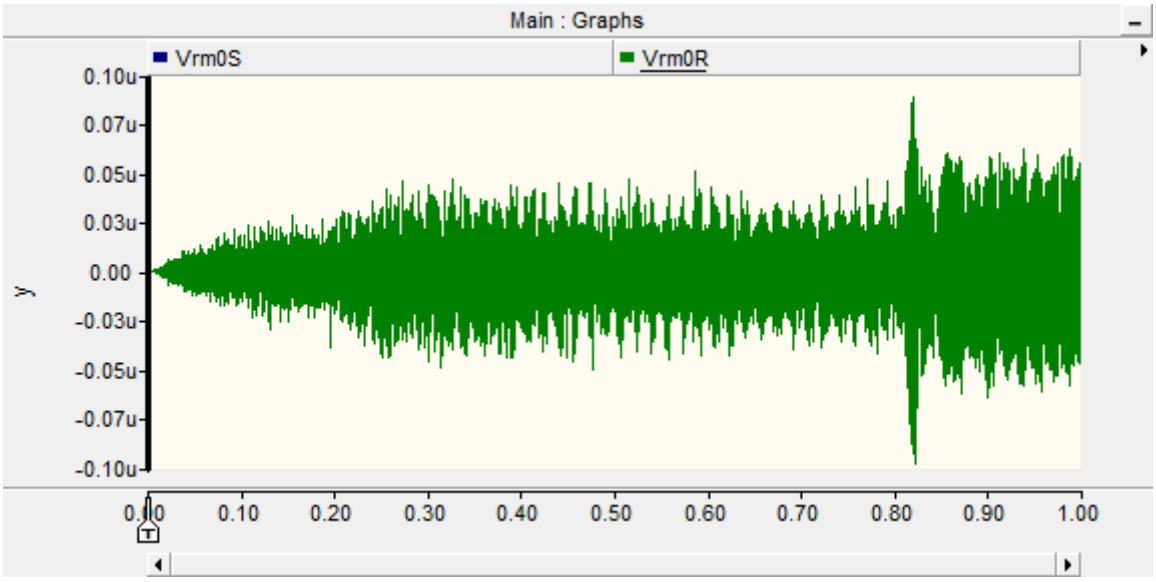

Figure 7.17 Mode 0 receiving end signal for a fault at the sending end after changing mutual inductance to 50uH for the hybrid (3-segment) VSC-HVDC system

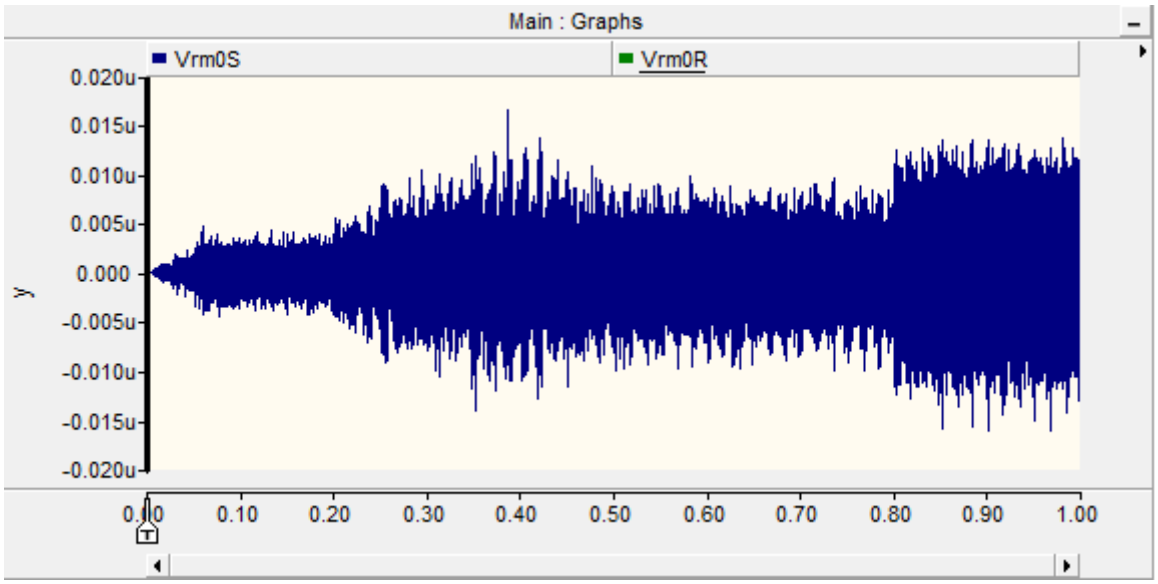

Figure 7.18 Mode 0 sending end signal for a fault at the sending end after changing the mutual inductance to 50uH for the hybrid (3-segment) VSC-HVDC system

The speeds of the wave were tuned again for better accuracy and it is found to be v_1=300000000 m/s for the overhead line and v_2=186200000 m/s for the cable. The results for this section is shown in Table 11. The maximum error percentage is %0.15 which is very small.

Table 11 Fault location results for the for the hybrid (3-segment) VSC-HVDC system using mode 1 signal

Fault location from sending end (km)	Calculated fault location (km)	Error (km)	Error (%)
1	1.67560	0.6756	0.0751
50	49.6760	0.3240	0.0360
150	150.176	0.1760	0.0196
300	301.971	1.9710	0.2190
400	399.726	0.2740	0.0304
450	450.000	0	0
600	598.029	1.9710	0.2190
650	649.324	0.6760	0.0751
750	751.324	1.3240	0.1471

8.0 CONCLUSIONS AND FUTURE WORK

A good method for fault location identification using transient data recorded on the terminals is critical for enhancing transmission system reliability and maintenance procedures, such as giving transmission line operators the opportunity to perform preventative maintenance. In addition, it will enable transmission line operators to perform maintenance economically and efficiently.

In this thesis, the traditional methods for fault location identification for different systems have been presented. Then the method for the VSC-HVDC system using Rogowski coil in [10] was applied and modified according to [6], to account for a hybrid transmission line consisting of both cables and overhead lines as shown in Figure 1.1 and Figure 1.2. The method was then tested on a non-hybrid and hybrid ideal DC source system, and then validated on a hybrid VSC-HVDC system with long lines (totaling 600 km for the 2-segment system and 900km for the 3-segment system). The method showed a maximum error of 0.23% for the hybrid 2-segment system and 0.15% for the hybrid 3-segment system.

This work provides a strong fondation for the fault location identification problem in VSC-HVDC systems and it can serve as the basis for the following future areas of investigation:

- Investigating the applicability of the algorithm on double faults and finding a modification that will account for this type of fault.
- Investigating ways to increase precision for the VSC-HVDC hybrid system, such as filtering and using Wavelet Transform methodology.

- Investigating and modifying the algorithm when current limiting reactors are added in the system.
- Investigating the fault location identification problem in Modular-Multi Level converter (MMC) systems with long non-hybrid and hybrid transmission mediums.

APPENDIX A

MATLAB CODE

A.1 THE HYBRID 2-SEGMENT SYSTEM CODE

```
%2-segments fault locator
%Mode 1 fault locator
clear all
c=0;


a=load('exp5_01.out'); %loading data for fault


t=a(:,1);
V1_1=a(:,5);
V2_1=a(:,4);

%The length of voltage vector
L_v1=length(V1_1);



%setting the threshold value based on analysis procedure done in the thesis
Thr=0.608;



%finding traveling wave arrival times at the two terminals. We start to
%scan for the first surge that exceeds the threshold starting from time 0.25
%s in order to neglect initialization transient period and false detection

k=0;
for n=(L_v1-1)/2:length(V1_1)-1
    if abs(V1_1(n))>=Thr
```

```
        k=k+1;
        n1(k)=n;
    end

end
t1=t(n1(1));
k=0;
for n=(L_v1-1)/2:length(V2_1)-1

    if abs(V2_1(n))>=Thr
        k=k+1;
        n2(k)=n;
    end

end

%calculating the difference between wave arrival times
t2=t(n2(1));
delta_t=t2-t1;
c=c+1;



%calculating the location of the fault measured from the right side station
using two
%terminal measurements

% setting the speeds of the traveling wave in the cable and overhead line
v1=187200000; %cable
v2=300000000 ; %overhead line

%the length of each segment 300km each
L1=300000; % Length of segment 1
L2=300000; %length of segment 2

%calculating the possible fault location distances from junctions, x1 and x2
X_f1=0.5*(L1+(v1/v2)*L2-delta_t*v1)/1000;
X_f2=0.5*(L2-(v2/v1)*L1-delta_t*v2)/1000;

%Determining the faulted segment and displaying the exact fault location
if X_f1<=L1/1000 &&  X_f1>=0
    f_location=X_f1;
    str1 = ['Fault is in section 1 (cable) at ',num2str(f_location),' km
measured from terminal 1'];
    disp(str1)
elseif X_f2<=L2/1000 &&  X_f2>=0
    f_location=X_f2+L1/1000;
    str2 = ['Fault is in section 2 (Overhead line) at ',num2str(f_location),'
km measured from terminal 1'];
    disp(str2)
else
    disp('Fault location cannot be determined')
end
```

A.2 THE HYBRID 3-SEGMENT SYSTEM CODE

```
%2-segments fault locator
%Mode 1 fault locator
clear all
c=0;


a=load('exp5_01.out'); %loading data for fault


t=a(:,1);
V1_1=a(:,5);
V2_1=a(:,4);

%The length of voltage vector
L_v1=length(V1_1);



%setting the threshold value based on analysis procedure done in the thesis
Thr=0.608;



%finding traveling wave arrival times at the two terminals. We start to
%scan for the first surge that exceeds the threshold starting from time 0.25
%s in order to neglect initialization transient period and false detection

k=0;
for n=(L_v1-1)/2:length(V1_1)-1
    if abs(V1_1(n))>=Thr
        k=k+1;
        n1(k)=n;
    end

end
t1=t(n1(1));
k=0;
for n=(L_v1-1)/2:length(V2_1)-1

    if abs(V2_1(n))>=Thr
        k=k+1;
        n2(k)=n;
    end
```

```
end

%calculating the difference between wave arrival times
t2=t(n2(1));
delta_t=t2-t1;
c=c+1;



%calculating the location of the fault measured from the right side station
using two
%terminal measurements

% setting the speeds of the traveling wave in the cable and overhead line
v1=300000000; %overhead line
v2=186200000;%cable
v3=300000000;%overhead line

%the length of each segment 300km each
L1=300000; % Length of segment 1
L2=300000; %length of segment 2
L3=300000; %length of segment 3

%calculating the possible fault location distances from junctions, x1, x2 and
x3
X_f3=L1/1000-((delta_t+L1/v1+L2/v2+L3/v3)*(v1/2))/1000;
X_f2=L2/1000-((delta_t-L1/v1+L2/v2+L3/v3)*(v2/2))/1000;
X_f1=L3/1000-((delta_t-L1/v1-L2/v2+L3/v3)*(v3/2))/1000;


 %Determining the faulted segment and displaying the exact fault location
if X_f1<=L1/1000 &&  X_f1>=0
    f_location=X_f1;
    str1 = ['Fault is in section 1 (Overhead line) at ',num2str(f_location),'
km measured from terminal 1'];
    disp(str1)
elseif X_f2<=L2/1000 &&  X_f2>=0
    f_location=X_f2+L1/1000;
    str2 = ['Fault is in section 2 (Cable) at ',num2str(f_location),' km
measured from terminal 1'];
    disp(str2)
elseif X_f3<=L3/1000 &&  X_f3>=0
    f_location=X_f3+L1/1000+L2/1000;
    str2 = ['Fault is in section 3 (Overhead line) at ',num2str(f_location),'
km measured from terminal 1'];
    disp(str2)
else
    disp('Fault location cannot be determined’)
end
```

BIBLIOGRAPHY

[1] “What the Smart Grid Means to America's Future: Technology Providers”, U.S. *DOE’s Office of Electricity Delivery and Energy Reliability*, 2008.

[2] “20% Wind Energy by 2030: Increasing Wind Energy's Contribution to U.S. Electricity Supply” *U.S. DOE: Energy Efficiency and Renewable Energy*, Jul. 2008

[3] Reed, G.F.; Al Hassan, H.A.; Korytowski, M.J.; Lewis, P.T.; Grainger, B.M., "Comparison of HVAC and HVDC solutions for offshore wind farms with a procedure for system economic evaluation," Energytech, 2013 IEEE , vol., no., pp.1,7, 21-23 May 2013

[4] "IEEE Guide for Determining Fault Location on AC Transmission and Distribution Lines," *IEEE Std C37.114-2004* , vol., no., pp.0_1-36, 2005

[5] Ke Jia; Thomas, D.; Sumner, M.; , "A New Single-Ended Fault-Location Scheme for Utilization in an Integrated Power System," *Power Delivery, IEEE Transactions on* , vol.28, no.1, pp.38-46, Jan. 2013

[6] Nanayakkara, O.M.K.K.; Rajapakse, A.D.; Wachal, R.; , "Location of DC Line Faults in Conventional HVDC Systems With Segments of Cables and Overhead Lines Using Terminal Measurements," *Power Delivery, IEEE Transactions on* , vol.27, no.1, pp.279-288, Jan. 2012

[7] Shang, L.; Herold, G.; Jaeger, J.; Krebs, R.; Kumar, A.; , "High-speed fault identification and protection for HVDC line using wavelet technique," *Power Tech Proceedings, 2001 IEEE Porto* , vol.3, no., pp.5 pp. vol.3, 2001

[8] Dewe, M.B.; Sankar, S.; Arrillaga, J.; , "The application of satellite time references to HVDC fault location," *Power Delivery, IEEE Transactions on* , vol.8, no.3, pp.1295-1302, July 1993

[9] Zhang Yi-ning; Liu Yong-hao; Xu Min; Cai Ze-xiang; , "A novel algorithm for HVDC line fault location based on variant travelling wave speed," *Electric*

Utility Deregulation and Restructuring and Power Technologies (DRPT), 2011 4th International Conference on , vol., no., pp.1459-1463, 6-9 July 2011

[10] Amila Nuwan Pathirana, " Travelling Wave Based DC Line Fault Location in VSC HVDC Systems" ,*The University of Manitoba* , Master's Thesis, 2012

[11] Yanfeng Gong; Mynam, M.; Guzman, A.; Benmouyal, G.; Shulim, B.; , "Automated fault location system for nonhomogeneous transmission networks," *Protective Relay Engineers, 2012 65th Annual Conference for* , vol., no., pp.374-381, 2-5 April 2012

[12] J. J. Grainger and J. William D.Stevenson, Power System Analysis, New York: McGraw-Hill Inc, 2003.

[13] M. J.Iskykowski and E.Rosolowski, Fault Location On Power Network, New York: Springer, 2010.

[14] HVDC for Beginners and Beyond, Areva T&D UK Limited, 2009.

[15] Y. Gong, M. Mynam, A. Guzman, G. Benmouyal and B. Shulim, "Automated fault location system for nonhomogeneous transmission networks," in *2012 65th Annual Conference for Protective Relay Engineers*, 2012.

[16] Allan Greenwood, Electrical Transients in Power Systems, Second edition, John Wiley & Sons, Inc. 1991

[17] Ramboz, J.D., "Machinable Rogowski coil, design and calibration," *Instrumentation and Measurement Technology Conference, 1995. IMTC/95. Proceedings. Integrating Intelligent Instrumentation and Control., IEEE* , vol., no., pp.329,, 24-26 April 1995

[18] Y. Maekawa; K. Watanabe; S. Maruyama ,"Research And Development Of DC +/- 500KV Etruded Cables" Cigre, 21-203, Session 2002 Japan

[19] Gustavsen, B.; Martinez, J.A.; Durbak, D., "Parameter determination for modeling system transients-Part II: Insulated cables," *Power Delivery, IEEE Transactions on* , vol.20, no.3, pp.2045,2050, July 2005

[20] Koo-yong Shin; Dong-Il Lee; Jae-seop Lim; Mun-no Ju; Kwang-ho Yang, "Design of the DC ±500kV full scale transmission test line in Gochang," *Transmission & Distribution Conference & Exposition: Asia and Pacific, 2009* , vol., no., pp.1,4, 26-30 Oct. 2009

[21] J. Duncan Glover , Mulukutla Sarma, "Power System Analysis and Design", 2nd edition, PWS Publishing Co., Boston, MA, 1994

[22] Bo, Z.Q.; Weller, G.; Redfern, M.A., "Accurate fault location technique for distribution system using fault-generated high-frequency transient voltage signals," Generation, *Transmission and Distribution, IEE Proceedings-* , vol.146, no.1, pp.73,79, Jan 1999

[23] Magnago, F.H.; Abur, A., "Fault location using wavelets," Power Delivery, IEEE Transactions on , vol.13, no.4, pp.1475,1480, Oct 1998

[24] Tawfik, M. M.; Morcos, M.M., "ANN-based techniques for estimating fault location on transmission lines using Prony method," *Power Delivery, IEEE Transactions on* , vol.16, no.2, pp.219,224, Apr 2001

[25] M. Joorabian, S. M. A. T.Asl and R. K. Aggarwal. “Accurate fault locator for EHV transmission lines based on radial basis function neural networks” *Electric Power Systems Research*, vol. 71, no. 3, pp. 195–202, Nov. 2004.